



Barite-bearing cap dolostones of the Taoudéni Basin, northwest Africa: Sedimentary and isotopic evidence for methane seepage after a Neoproterozoic glaciation

Graham A. Shields ^{a,*}, Max Deynoux ^b, Harald Strauss ^a,
Hélène Paquet ^b, Daniel Nahon ^c

^a Geologisch-Paläontologisches Institut und Museum, Westfälische Wilhelms-Universität Münster,
Corrensstrasse 24, 48149 Münster, Germany

^b Ecole et Observatoire des sciences de la Terre, Centre de Géochimie de la Surface, CNRS-Université Louis Pasteur,
1 rue Blessig, 67084 Strasbourg Cedex, France

^c CEREGE, CNRS-Université d'Aix-Marseille III, BP 80, 13545 Aix-en-Provence, France

Received 24 May 2006; received in revised form 14 November 2006; accepted 22 November 2006

Abstract

The Taoudéni Basin of the West African craton contains one of the few genuine terrestrial records of a Neoproterozoic ice age. In the Adrar region of Mauritania, an extensive permafrost landscape, lithified moraines (tillites) and striated pavements are draped by a thin, generally <5-m thick dolostone, which is lithologically and isotopically similar to other basal Ediacaran cap dolostones worldwide. In Adrar, the cap carbonate unit exhibits a complex depositional history with significant lateral facies variation related to the irregular post-glacial, topographic relief and the complex interplay between glacioeustasy and isostatic rebound. The Adrar cap carbonate package consists of one or two dolostone units, with an intervening siliciclastic package of up to 40 m thickness, and a laterally extensive, thin limestone bed that disconformably overlies the uppermost dolostone. The cap dolostone comprises mechanically laminated beds that are disrupted by fitted-brecciation, sheet cracking, tepee formation, karstic dissolution and chaotic vein networks of silica, calcite and barite. The overlying thin bed of limestone breccia comprises volcaniclastic and detrital debris and authigenic barite crystals, cemented and commonly replaced by marine calcite. The close association between relative sea-level changes, glacier retreat and cap dolostone deposition across the Taoudéni Basin implies that cap dolostones formed largely over a period of $\sim 10^4$ years, the maximum interval over which isostatic rebound is likely to operate.

Barite has been reported from identical stratigraphic levels overlying terrestrial glacial deposits throughout NW Africa and formed locally during fluid mixing on, and in cavities beneath the seafloor during late stages of the post-glacial marine transgression. Samples of barite were collected from two distant localities in the Taoudéni Basin, in Mauritania and Mali. $^{87}\text{Sr}/^{86}\text{Sr}$ ratios exhibit an unusually narrow range for barite that closely matches contemporaneous seawater $^{87}\text{Sr}/^{86}\text{Sr}$ (0.7077–8). Barite $\delta^{34}\text{S}$ values range widely between 20‰ and 45‰ CDT, which indicates that sulphate derived from seawater and was subsequently modified by microbially mediated sulphate reduction. The consistent stratigraphic level and irregular distribution of barite deposits are consistent with a sedimentary exhalative origin for the barite, whereby Ba-rich fluids from shallow locations within the rock pile interacted with sulphate-bearing seawater; a hydrothermal origin for these fluids can be excluded. Isotopic constraints and the association of barite with terrestrial glacial deposits across the West African craton suggest that methane seepage from underlying permafrost may be one possible mechanism for Ba sequestration. The occurrence of seafloor barite precipitates at the contact between cap

* Corresponding author. Tel.: +49 251 83 33937; fax: +49 251 83 33925.
E-mail address: gshields@uni-muenster.de (G.A. Shields).

dolostones and overlying post-glacial limestones worldwide implies that changes in ocean composition, in particular increases in the sulphate content of ambient seawater provided an overriding control on barite mineralisation.

© 2006 Elsevier B.V. All rights reserved.

Keywords: Neoproterozoic; Cap carbonates; Methane seeps; Barite; Stable isotopes

1. Introduction

The West African craton provides sedimentological evidence for two episodes of glaciation that occurred during the Neoproterozoic and Late Ordovician. The Late Ordovician glaciogenic deposits relate to the Hirnantian episode of global cooling around 440 Ma, while the Neoproterozoic deposits most likely correspond to the unusually extensive, late Cryogenian Period *Elatina* ice age (commonly referred to as Marinoan), which is thought to have ended around 635 Ma (Condon et al., 2005). The apparently world-wide extension of ice sheets during parts of the Cryogenian Period (ca. 750–635 Ma) implies either global refrigeration with glaciers at sea-level even at equatorial latitudes (Harland, 1964; Evans, 2000), or rapid plate movement, which left a trail of diachronous tillites (Crawford and Daily, 1971; Deynoux et al., 1978; Crowell, 1983). Recently, support for equatorial ice sheets has been growing with new paleomagnetic evidence from Neoproterozoic glaciogenic successions in Australia (Sohl et al., 1999) and Oman (Kilner et al., 2005).

The close association of glacial deposits with sediments more characteristic of a tropical climate regime, such as dolostone or ironstone, is typical of most Neoproterozoic glaciogenic successions, as well as the NW African deposits concerned here, and this enigma has been discussed at length in the literature (e.g. Schermerhorn, 1974; Williams, 1975; Deynoux and Trompette, 1976; Young, 1976; Fairchild, 1993; Hoffman et al., 1998). Marine carbonates, sometimes stromatolitic and oolitic, occur within or below Cryogenian Period tillites and glaciogenic diamictites in Australia and Mauritania (Fairchild, 1993) and above them in Mauritania (Trompette, 1973) and worldwide (Kennedy et al., 1998; Hoffman and Schrag, 2002). Although carbonate deposition is not everywhere associated with warm waters today, cold-water carbonate deposition seems less probable in the Precambrian marine environment due to the absence of active CaCO_3 biomineralisation by animals (Shields, 2005).

The association of carbonate and glaciogenic strata indicates that climatic fluctuations were both extreme and abrupt (Spencer, 1971; Wilson and Harland, 1964; Fairchild, 1993) and/or that saturation states were unusu-

ally high (Spencer and Spencer, 1972; Ridgwell et al., 2003). Rapid warming after glaciation would be consistent with the equatorial latitudes of many glacial deposits and forms an essential feature of the Snowball Earth hypothesis (Hoffman et al., 1998). However, no paleotemperature proxies have been able to test this idea as yet. Possible calcite pseudomorphs of ikaite (glenodinite), which is a cold-water form of calcium carbonate, have been reported from pre-glacial, oolitic carbonate rocks of NW Canada (James et al., 2005). The precipitation of ooids under apparently cold conditions implies that carbonate saturation levels may have been high even at low temperatures during parts of the Neoproterozoic, although again this finding is equally compatible with extreme climate fluctuations.

It lies outside the scope of this paper to discuss the origin of all cap carbonates around the world and we instead refer the reader to published reviews (James et al., 2001; Hoffman and Schrag, 2002; Shields, 2005). Below we restrict our discussion to field, petrographic and geochemical data that directly bear on the origin of the very extensive barite-bearing, calcareous dolostone horizon that caps glaciogenic Neoproterozoic deposits of the Taoudéni Basin in West Africa. In particular, we focus on the genesis of the barite, which is enigmatically restricted to the cap dolostone horizon throughout the Taoudéni Basin. We discuss our model in the light of other barite occurrences in cap dolostones from the neighbouring Volta Basin, and from some other localities worldwide (Hoffman and Schrag, 2002; Jiang et al., 2003). Recently, Sr and S isotope constraints have been used to distinguish between the various types of sedimentary exhalative and stratiform barite deposits (Maynard et al., 1995; Jewell, 2000; Clark et al., 2004; Torres et al., 2003). Here, we apply these constraints, isotope stratigraphy and sedimentological criteria to the stratiform barite deposits of Mauritania and Mali in order to constrain the age, duration and genesis of post-glacial strata from West Africa.

2. Geological setting

The West African craton has been a tectonic entity since at least 1600 Ma and is rimmed by mobile belts that became active during Late Proterozoic and Paleo-

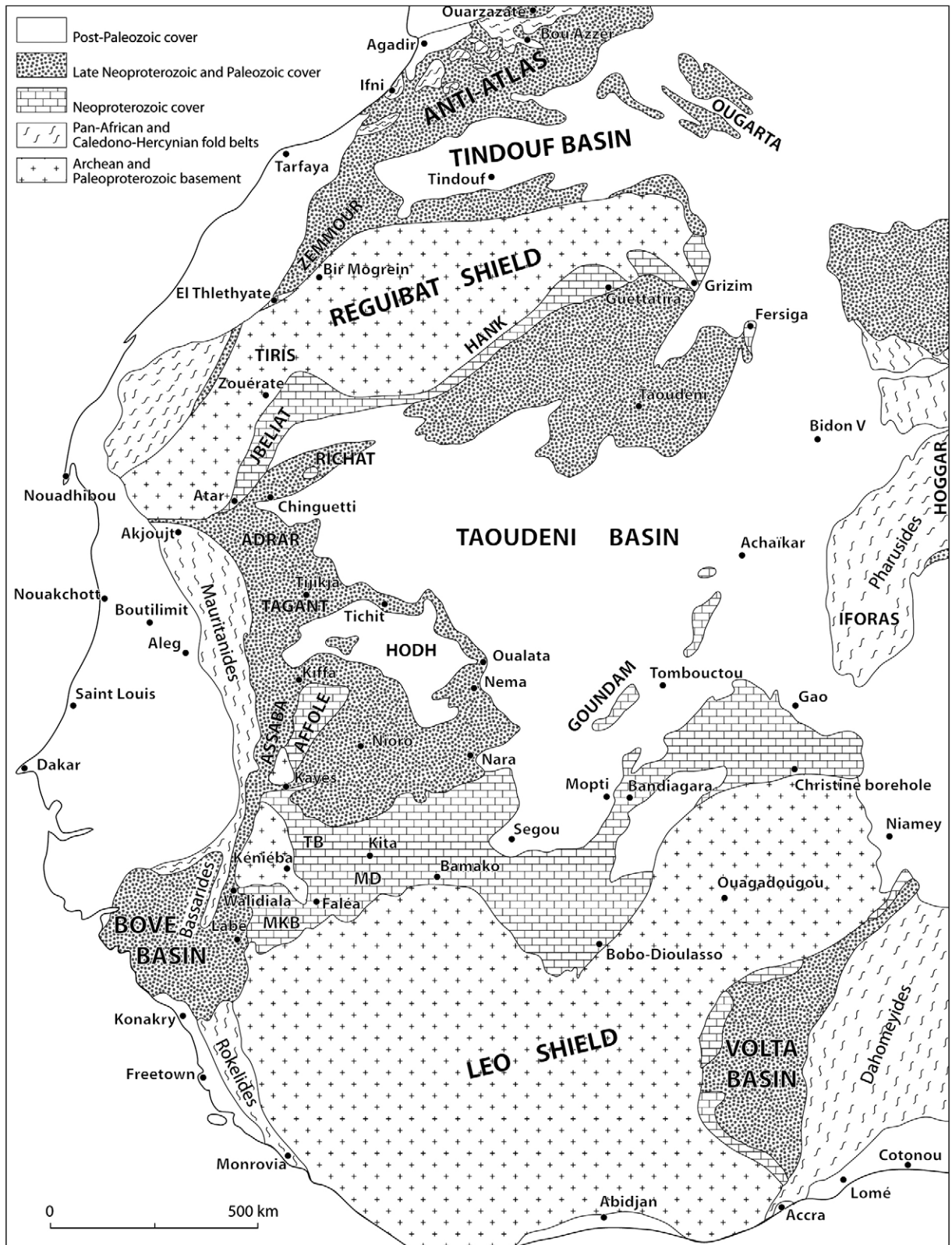


Fig. 1. Simplified geological map of the Taoudéni Basin and adjacent areas in NW Africa.

zoic times (Fig. 1). On the craton, the sedimentary cover is preserved in widespread, variably connected basins containing Upper Proterozoic and Paleozoic deposits. The largest of them, the Taoudéni Basin with which we are concerned here, forms a thin (3 km on average), continuous tabular blanket over distances of 1000–1500 km (Fig. 1).

With the exception of the area fringing the peripheral fold belts, the Taoudéni Basin has only been affected by epirogenic movements, which generated low angular unconformities, and the reactivation of basement faults frequently injected by diabases. The sedimentary deposits are generally devoid of tectonism, while metamorphism is limited to the thermal effects of diabase intrusions in the proximal host material that took place during the opening of the Atlantic Ocean during the Jurassic Period. In this regard, it has been demonstrated (Girard, 1985; Girard et al., 1989) that some sediments experienced locally high-grade, hydrothermal diagenesis. In spite of their age, the sediments have undergone only modest burial diagenesis because the sedimentary pile is relatively thin and the platform has remained above sea-level since the end of the Carboniferous Period.

The stratigraphic type-section of the Taoudéni Basin was established by Trompette (1973) in the Adrar region of Mauritania (Fig. 2), where the dolostone unit that caps the glacial deposits was sampled for this study. Preglacial sediments of the Adrar part of the Taoudéni Basin (Mauritania) are characterized by marine sediments, including diverse stromatolites of the Atar Group (Fig. 3), which Rb/Sr and K/Ar isotope studies of clay minerals has dated to the Early Neoproterozoic (Clauer, 1976; Clauer et al., 1982). Strontium isotope constraints are consistent with this interpretation (Veizer et al., 1983; Shields, 2002). The Atar Group and overlying siliciclastic rocks of the Assabet-el-Hassiane Group were tilted slightly by Pan-African events before being peneplaned by subsequent uplift and erosion to form a largely flat, sub-glacial substrate (Deynoux, 1980).

The glacial units and “cap dolostone” form the Jbeliat Group (Deynoux, 1980), which lies with angular and erosional unconformity either on the lower part of the sedimentary succession (Fig. 2) or directly on the basement. The Jbeliat Group is overlain by bedded cherts, green shales and siltstones of the Téniagouri Group. The lithostratigraphic Triad association: “diamictite-dolostone-bedded chert” has long been used as a marker

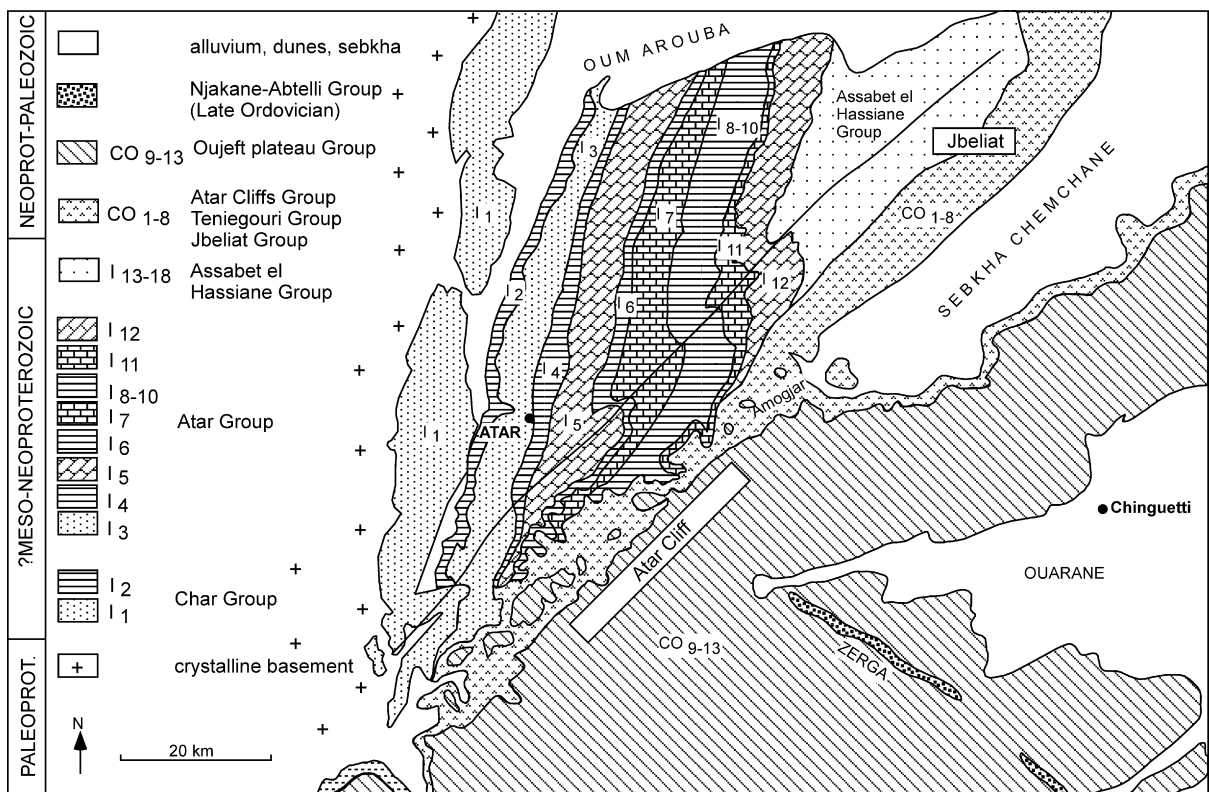


Fig. 2. Geological sketch map of the Atar Cliff and Jbeliat areas of the Adrar region (after Trompette, 1973).

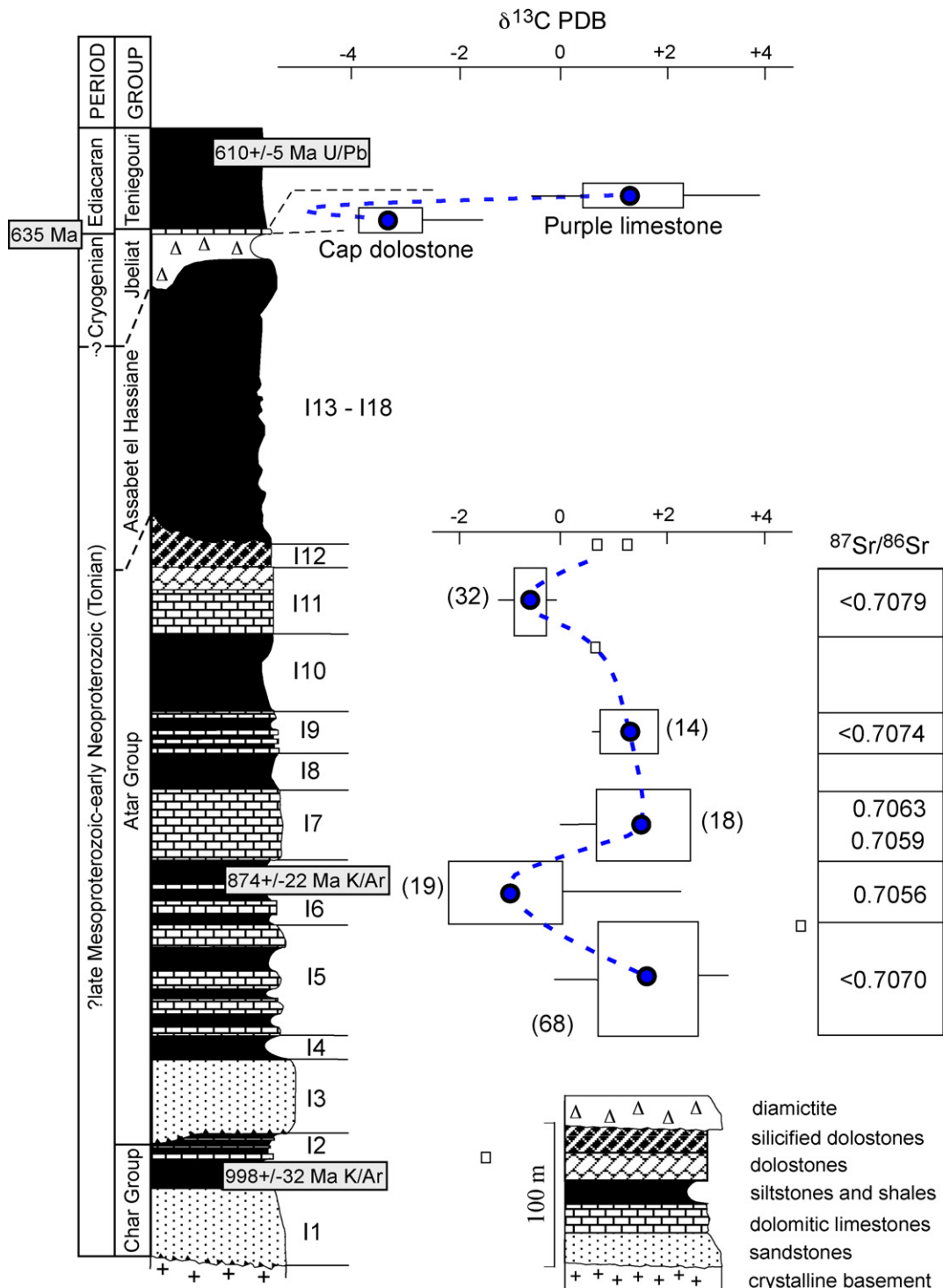


Fig. 3. Simplified stratigraphic log and Sr- and C-isotope stratigraphy of the preglacial Atar Group and glacial Jbeliat Group based on data from Tables 1 to 4 and published $\delta^{13}\text{C}$ (Fairchild et al., 1990; herein) and $^{87}\text{Sr}/^{86}\text{Sr}$ (Shields, 2002, unpublished results) data. Box symbols show whole range (horizontal lines), standard deviation (box limits) and average values (black circles) of sample sets (number of individual samples from each formation shown in brackets). Small boxes refer to individual samples. $^{87}\text{Sr}/^{86}\text{Sr}$ values refer to least altered ratios in each case, and therefore a closest approximation to contemporaneous seawater. Age constraints are from Lahondère et al. (2005) and Clauer et al. (1982). Six hundred and thirty five Ma is a suggested age based on global correlation schemes.

horizon in the Taoudéni Basin (Zimmermann, 1960) as well as in the adjacent Volta Basin (Leprun and Trompette, 1969). The characteristics and palaeogeographic distribution of the paleo-glacial drift have been described elsewhere and are synthesized in Deynoux and Trompette (1981), Deynoux (1985) and Deynoux et al. (2006).

Because the only chronostratigraphically useful fossils have been found in overlying Silurian shales (Oued Chig group), a late Neoproterozoic age was deduced for the glacial deposits solely on the basis of Rb-Sr and K-Ar isotopic studies of clay minerals in overlying and underlying formations (Clauer et al., 1982; Clauer and Deynoux, 1987). Specifically, the Jbeliat Group tillite is considered to correspond to the late Cryogenian (Elatina/Ghaub/Nantuo) glacial period, which is now known to have ended at about 635 Ma (Condon et al., 2005). A late Neoproterozoic age is consistent with the presence of stromatolites and acritarchs in the preglacial sequences because of their similarity to those from Riphean successions of Russia (Bertrand-Sarfati and Trompette, 1976; Porter et al., 2004). Although reports of Early Cambrian small shelly fossils in cap dolostones from the southwestern part of the basin (Culver et al., 1988; Culver and Hunt, 1991) were initially taken to indicate a Cambrian age for the Taoudéni Basin triad (Bertrand-Sarfati et al., 1995; Evans, 2000), a reassessment of those previous fossil reports and new stable isotope data (Porter et al., 2004; Shields et al., in press) provide further support for a Neoproterozoic age. Two U-Pb zircon ages have recently been reported for two volcanic tuffs of the Ténigouri Group that directly overlie the Jbeliat Group in Mauritania (Lahondère et al., 2005). These new age constraints (609.7 ± 5.5 Ma, U/Pb zircon and 604 ± 6 Ma, U/Pb SHRIMP) effectively rule out a Cambrian age for the Taoudéni Basin triad and are consistent with the postulated 635 Ma age. These new results add further evidence for the globally correlative nature of cap dolostones, and by implication deglaciation, at the end of the Cryogenian Period.

Carbonate rocks are otherwise uncommon in the post-glacial sedimentary record of Adrar and are only represented by a thin level of purple limestone at the very base of the Ténigouri Group and by a thin silicified, stromatolitic dolostone bed within the basal part of the overlying Atar Cliff Group (Trompette, 1973). The cap dolostone is present across the platform but thins to zero towards the fold belts, which were deeper oceanic troughs during the glacial period. Barite is a consistent feature of the cap dolostone on the margins of the Taoudéni Basin where terrestrial periglacial deposits dominate the glaciogenic successions.

3. Field descriptions, petrography and mineralogy

In the Taoudéni Basin, the cap carbonate unit generally occurs as a single persistent stratigraphic horizon 3–5-m thick (Fig. 4) but occasionally splits into two thin units separated by a siliciclastic package up to 40 m in thickness (Fig. 4). The cap dolostone rests unconformably either on the glacial deposits or in places directly on the preglacial substrate. In the northern part of the basin, the Jbeliat Group outcrops along a nearly continuous 1300 km long narrow belt from the Adrar region to the north-eastern limit of the Hank region in Algeria (Fig. 1). Along this belt, the glacial drift comprises just a few metres of terrestrial tillite, with polygenic and often striated pebbles to boulders, overlying striated pavements. Locally, a complex facies association is preserved in smooth large-scale paleodepressions such as in the Jbeliat area in Adrar (Fig. 4). In these paleodepressions, the glacial deposits thicken up to 50 m and comprise distinct glacial sequences suggesting at

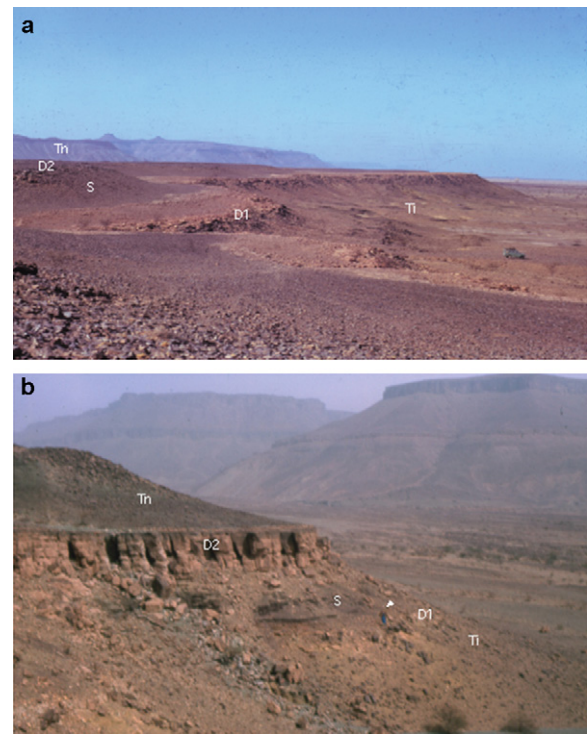


Fig. 4. Views of the Jbeliat Group in the Jbeliat area (a) and along the Atar cliff (b). In these exposures, the glacial deposits (Ti), are overlain by two horizons of cap dolostone (D1 and D2) separated by purple shale (S), and in turn overlain by bedded cherts and shales of the Ténigouri Group (Tn). In (b), D2 consists of 7-m thick scarp of cross-bedded carbonaceous sandstones and conglomerates. Vehicle in (a) and person (arrow) in (b) for scale.

least three glacial events, with terrestrial tillites, outwash sandstones and various glacial features, such as striated clasts and pavements, roches moutonnées, lacustrine varves with dropstones, and remarkable polygonal structures and sand wedges related to permafrost just below the cap dolostone (Deynoux and Trompette, 1976; Deynoux, 1980, 1982, 1985). These deposits represent probably one of the only well-preserved, purely continental records of a Pre-Pleistocene ice sheet (Eyles and Januszczak, 2004).

The following descriptions concern the cap dolostone of these northern regions of the Taoudéni Basin, in Adrar, along a 100 km long nearly linear exposure of the Triad (Fig. 2), where it forms an easily traceable scarp in the tabular Jbeliat area in the north (Fig. 4a) and southward along the Atar cliff (Fig. 4b). However, the main characteristics can also be applied to the cap dolostone in other parts of the basin. In Adrar, the cap carbonate package can be divided into three distinct lithostratigraphic units: (1) the cap dolostone (facies Ixa: Deynoux, 1980); (2) a siliciclastic unit that intervenes between two thin hori-

zons of cap dolostone in places (facies Ixb: Deynoux, 1980); (3) an overlying thin, but persistent horizon of purple limestone (facies TXc: Deynoux, 1980). Detailed sections can be found in Deynoux (1980, 1985) and so are not reproduced here. Our petrographic studies involved standard light-microscopy of over 100 thin-sections, X-ray diffraction analyses of the clay (<2 µm) fractions and confirmatory semi-quantitative elemental analyses using scanning electron microscopy.

3.1. Cap dolostone

The generally buff-coloured cap dolostone is either well-bedded or brecciated (Fig. 5). The well-bedded facies consists of alternating centimetric- to decimetric-scale beds, often with thin and discontinuous intervening stringers of black chert. Alternating cream and brown colour-banding is associated with grain-size contrasts between beds. Bedding surfaces are commonly erosional at all scales, i.e. scoured, rather than gradational or crinkled as with microbialites. Generally internally massive,

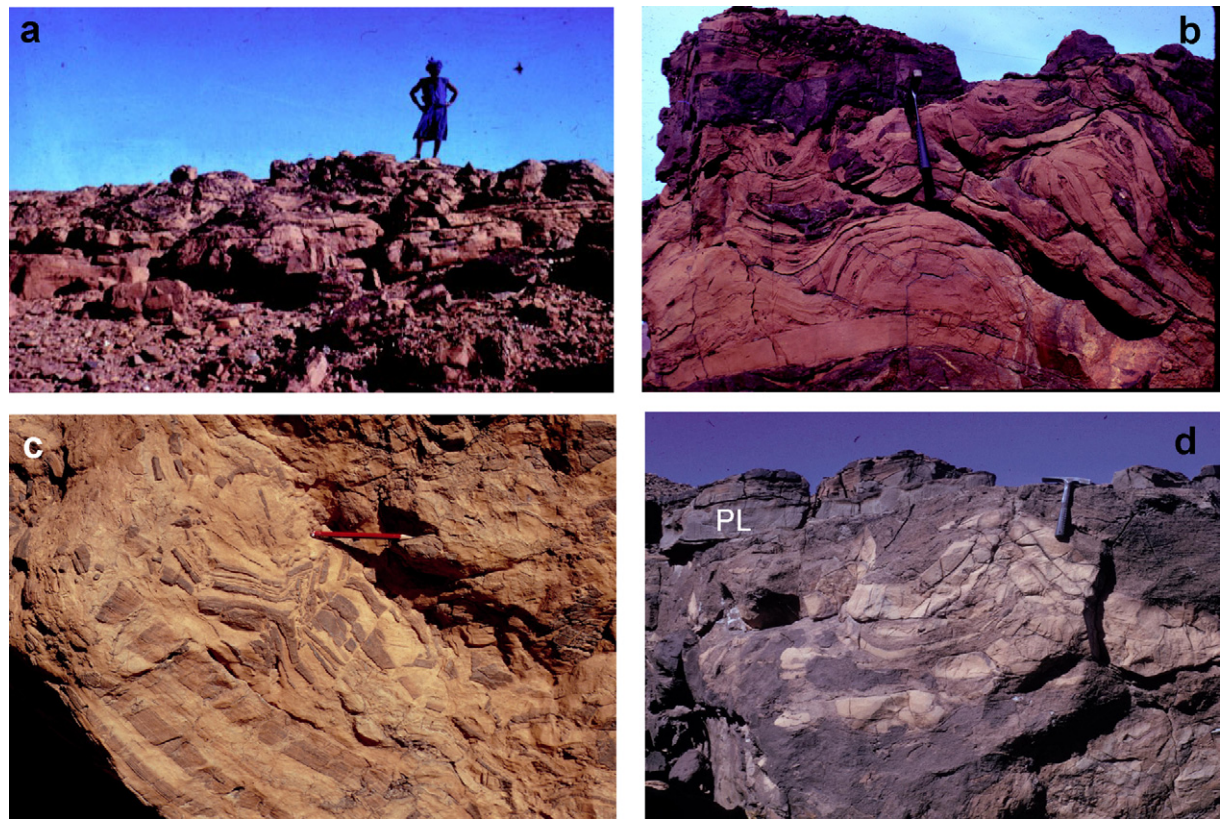


Fig. 5. (a) Bedded (lower part) and brecciated (upper part) aspects of the cap dolostone in the Jbeliat area. (b and d) Ductile and brittle arching giving way to dome or teepee-like structures. PL in (d) corresponds to a persistent 30-cm thick horizon of purple limestone overlying the cap dolostone. Note the numerous cracks filled with black chert, which cut the dolostone beds in (b). Well defined cap dolostone beds in (c) pass laterally and vertically into fitted brecciated and buckled facies.

they may display flat or wavy laminations, and minor cross-bedding. No microbial textures have been recognised, but microbial, dolomitic and apatitic stromatolites have been observed within the cap dolostone in the Algerian part of the Hank (Fig. 1) (Bertrand-Sarfati et al., 1997), as well as in the southern part of the basin in Western Mali (Rossi, 1982).

The brecciated facies can be located at various levels within the cap dolostone, although generally not at the base, and the passage between the two facies is progressive. When passing to the brecciated facies, beds become laterally and vertically folded and disrupted (Fig. 5). Ductile or brittle arching gives way to domed or more angular tepee-like structures, and boudinage (Fig. 5). Folded structures, such as overturned folds and upward buckling of broken pieces have also been observed. In extreme cases, angular pieces of chaotically oriented cream dolostone are found entirely isolated in a brown dolomitic matrix rich in black chert, millimetric-scale idiomorphic quartz and barite. Fissures are common and are generally filled with ferroan dolomite, black chert, white quartz or barite. A second generation of fissures is filled with very coarse, ferroan calcite spar.

Barite (Fig. 6), which is associated with the brecciated facies, appears as palisadic crystals filling cracks or cavities, as well as monocrystalline geodes and laminated domes up to 30 cm across showing the characteristic isopachous layering of chemical precipitates (Fig. 6e). Digitate barite columns are commonly separated by calcite spar at Jbeliat, while twinned barite crystals retain inclusions of chert and calcite along twinning planes and along growth bands. Iron oxide minerals are abundant as are reddish brown, isotropic patches, which could be phosphatic collophane. Barite in the upper dolostone is found in places to encrust vein-fed cavities (Fig. 6f) filled with calcitic spherulites that coarsen upward from 1 mm to several cm across (see purple limestone below). Spherulite contacts are polygonal due to interference and clearly grew in place. Spherulites frequently contain an irregularly shaped core of greenish, amorphous material (isotropic under polarised light), which is interpreted as devitrified glass.

In the Jbeliat area, an isolated dome of brecciated dolostone, 1.5 m high and 4 m in diameter, protrudes above the lower dolostone horizon (Fig. 6b). The surrounding dolostone beds are curved upward against the dome, which is draped by the intermediate purple shales. Larger, but more shallowly dipping domes (up to 4 m high and 20 m wide) were observed in the same area (Fig. 6a and d) in a zone where the cap dolostone forms a single horizon. These domes are onlapped by the bedded cherts of the Ténigouri Group (Fig. 6a), while one

of them is characterized by the presence along its flanks of isolated or amalgamated balls (10–70 cm in diameter) of barite (Fig. 6c and d). Some of these balls seem to have formed on the sea-floor before rolling down the flanks of the dome.

Microscopically, the cap dolostone comprises alternating grain sizes from dolomicrite to dolosparite with poorly developed or residual cement made up of a mixture of clay, cryptocrystalline silica, siderite and pyrite. Dolomite crystals are iron-rich and their borders tinged with the brown of oxidised iron. In certain cases, dolomite crystal mosaics resemble the “chicken-wire” structure that is indicative of gypsum pseudomorphs. The clay fraction was separated and shown to comprise detrital kaolinite (10–20%) and illite (20–40%) as well as diagenetic palygorskite (10–20%) and smectite (20–40%).

3.2. Siliciclastic unit

The cap dolostone splits locally into two distinct stratigraphic horizons providing room for up to 40 m of onlapping green to purple shales and siltstones including sandy dolostone intercalations. Along the Atar cliff, the upper dolostone horizon becomes progressively sandy until it forms a bank up to 7-m thick (Fig. 4b) made up entirely of coarse-grained to granular, trough cross-bedded, dolomitic sandstone (Fig. 7c) with isolated lenses of finer dolostone (Fig. 7d). In the transition zone, the sandy material fills irregular and variously oriented fissures within the dolostone; in places angular pieces of dolostone are isolated within the sandstone. Detrital elements within the siliciclastic unit are represented by rounded to angular quartz grains, rare feldspars (oligoclase, microcline, perthite), ferruginous minerals (magnetite, oxidised pyrite, haematite), which can be as abundant as quartz, and abundant mica (muscovite, biotite, chlorite). Muscovite is ubiquitous, whereas biotite is not always present, having commonly undergone chloritisation or ferruginisation. The cement generally consists of dolospar and dolomicrospar, but may also comprise barite and chlorite, goethite and haematite, or clay minerals: mostly illite with traces of chlorite and/or kaolinite and more rarely smectite. The dolomitic cement was the last to form and envelopes all the other cement types as well as the detrital grains.

3.3. Purple limestone

In the Jbeliat area and part of the Atar cliff area, over about 30–40 km of the cap dolostone exposure, a persis-

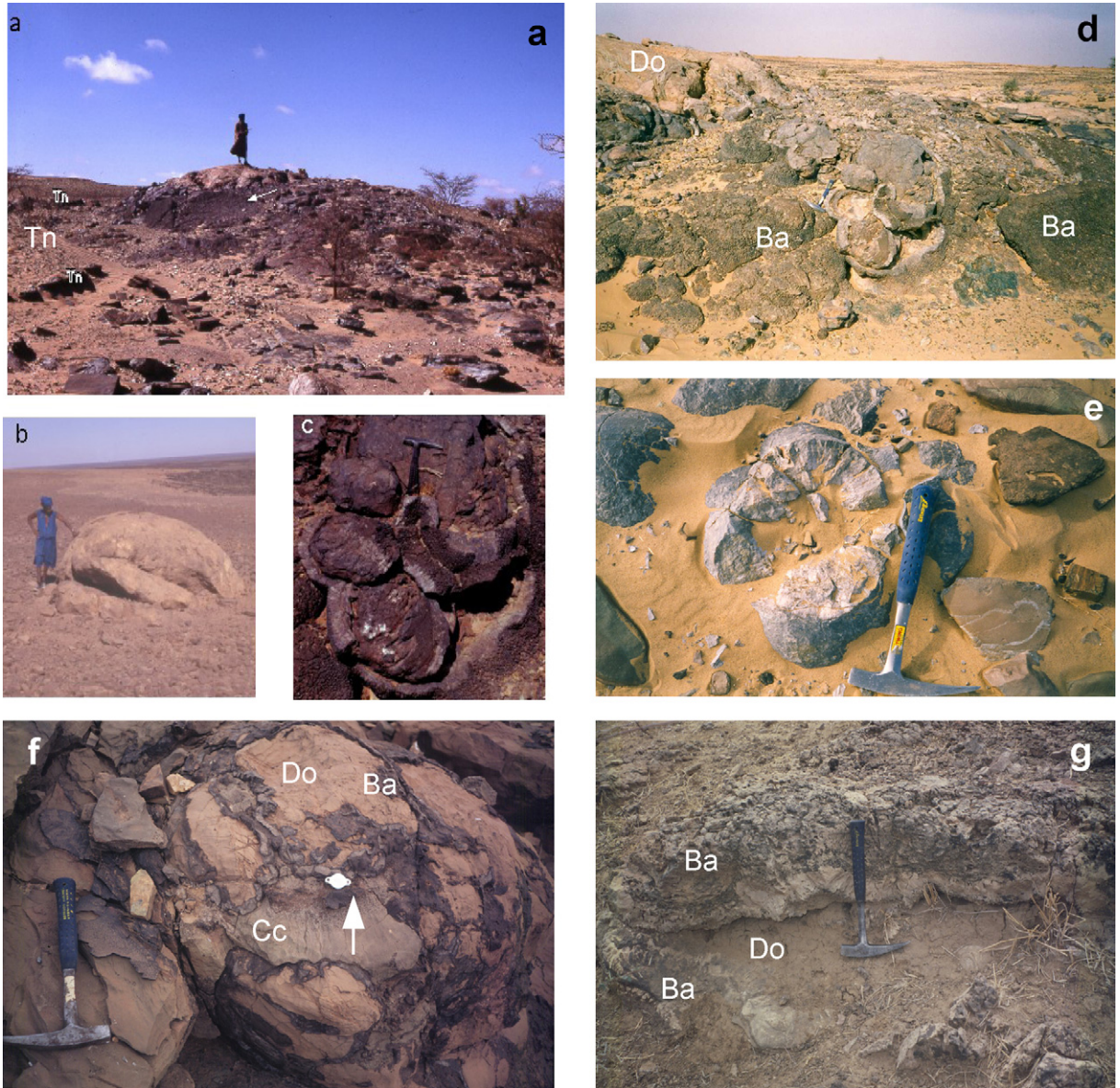


Fig. 6. Large protruding domes of cap dolostone in the Jbeliat area (a), (b) and (d). The surrounding dolostone beds are curved upward against the domes, which are onlapped by either the intermediate purple shales in the case of lower dolostone domes (b) or by bedded cherts of the Ténigouri Group (Tn and arrow in a). In (d), barite (bluish grey where fresh and dark grey where exposed) drapes domes and forms balls with massive cores and digitate rims (c) as well as isopachous mamelons (e). Veins of barite (Ba) coat walls of a cavern within the upper of two cap dolostone (Do) units in the Atar Cliff area (f); caverns are filled with reverse-graded (shown by arrow), calcitic nodules (Cc) and devitrified volcanic glass fragments. Barite at Pont de Kabate, Mali (g) shows similar features to Jbeliat forming digitate chemical precipitates and filling fissures (For interpretation of the references to colour in this figure legend, the reader is referred to the web version of the article.).

tent 30–50-cm thick horizon of limestone is intercalated between the cap dolostone and bedded cherts/siltstones of the overlying Ténigouri Group. It is characterized by its purple to grey-green colour and its breccia texture defined by oriented, millimetric- to centimetric-scale, angular flakes of dark red siltstone or chert (Fig. 8a) and millimetric-scale dark to greenish, irregularly shaped,

black-rimmed bodies. At both Jbeliat and the Atar Cliffs area, this calcitic horizon may comprise millimetric-sized, reverse-graded, calcitic nodules or spherulites (Fig. 8d), which in the Atar Cliffs area are found either to sharply overlie disrupted cap dolostone directly (Fig. 5d) or conglomeratic, cross-bedded, dolomitic sandstone which erosively overlies the cap dolostone in places



Fig. 7. Upper, disrupted part of the cap dolostone in the Atar cliff area (a) and (b) passing progressively into conglomeratic, cross-bedded sandstone with sand-filled cracks; note the thin lenses of dolomite at this level. The sharp contact on which the hammer head is resting in (a) marks a flooding surface and likely hardground that is overlain by an unusually thick 50 cm layer of calcite nodules and greenish devitrified glass and shales (correlative layer to the purple limestone in Fig. 5d). Along strike, the sandy level (c) and (d) can be up to 7-m thick and forms part of the upper cap dolostone unit (D2 in Fig. 5b), which is here entirely made up of trough cross-bedded carbonate-rich sandstone (c) with dolostone lenses (d) (For interpretation of the references to colour in this figure legend, the reader is referred to the web version of the article.).

(Fig. 7a and b). The stratigraphic level and conglomeratic aspect of these conglomeratic beds and the presence of dolomite lenses (cf. Fig. 7a–d) confirm that this level is equivalent to the upper cap dolostone in parts of the Atar Cliffs area where two levels are found. These calcitic nodules often reveal a translucent, green core and are identical to the above-mentioned spherulites that were found to fill barite-coated caverns within upper levels of the cap dolostone (Fig. 6f). The crystal spherulites consist of monocrystalline calcite with sweeping extinction. Where present the cores consist of polycrystalline quartz. Mixed in with the nodules are partially corroded, green-coloured laths of amorphous silicate and polycrystalline quartz, which are interpreted to be the altered remnants of volcanic glass.

In thin-section, the purple limestone unit at Jbeliat consists largely of sparry calcite that cements flake-like

clasts of siltstone and chert, and dispersed, black-rimmed bodies of highly variable shape (from rounded or ovoid, to flake-like, acicular or shard-like). Their black rims consist of agglomerations of tiny ($<1\text{ }\mu\text{m}$) iron oxy-hydroxides. Internally, they consist of authigenic quartz or a mixture of green clay minerals, including chlorite and glauconite/celadonite, the last two minerals being impossible to distinguish using X-ray techniques alone. The glauconite/celadonite assemblage can make up all of the blob interior, but is more frequently replaced by chlorite in the form of small bundles up to larger fans, whose orientations are normal to the black rim. Between these fans, voids are occupied by barite crystals (Fig. 8b), as monocrystals or assemblages of intergrown euhedral crystals that contain bundles of chlorite as inclusions and have clearly grown over the chlorite precursor mineral, i.e. glauconite-celadonite (Fig. 9).

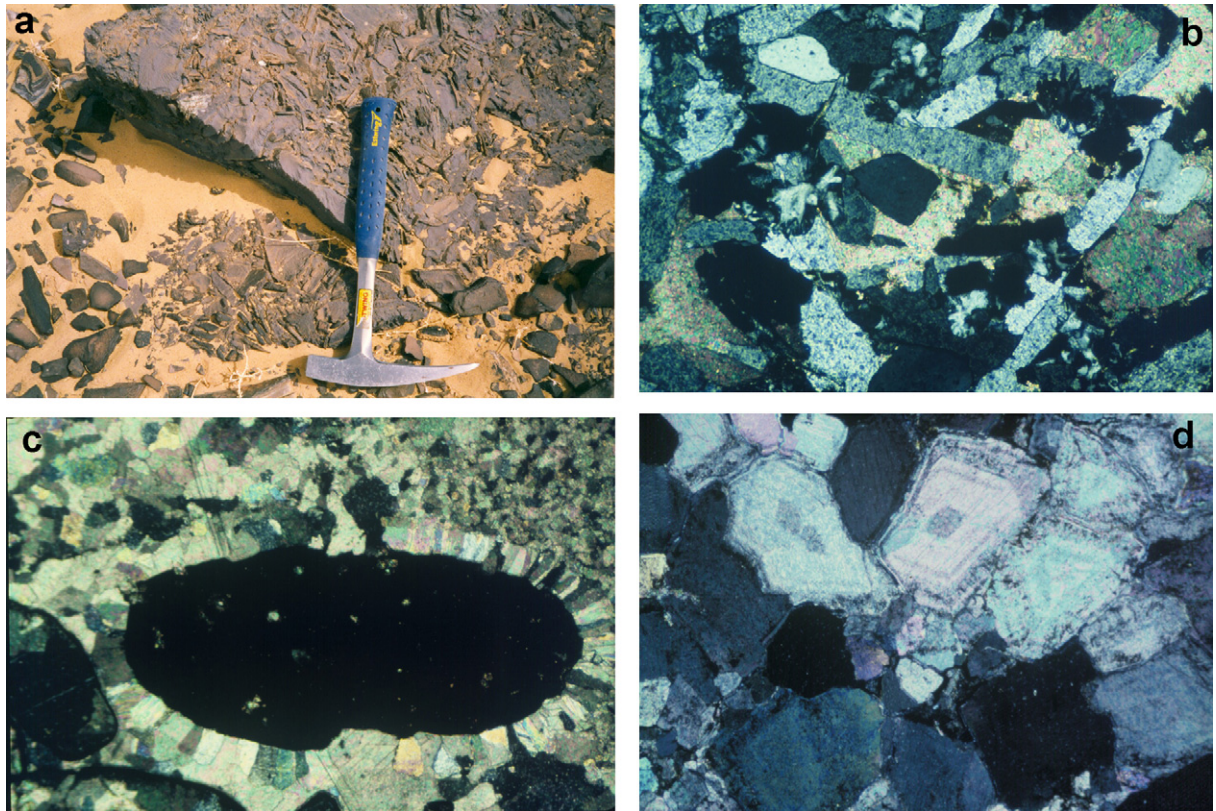


Fig. 8. Flake breccia of the purple limestone at Jbeliat (a). In thin-section, flakes are amorphous, isotropic silica-rich bodies of devitrified glass cemented by marine calcite (c) with euhedral barite crystals partially replaced by calcite (b). The correlative calcite nodule layer (d) of the Atar Cliff area contains volcaniclastic debris between and within spherulite cores.

Other automorphic minerals may be observed in paragenetic association with barite, such as small twinned crystals of euhedral albite that are arranged in small nests epitaxically developed on barite. Otherwise, some black-rimmed bodies may be occupied by monocrystals of automorphic or xenomorphic quartz that follow the interior surfaces of the blobs. Besides these black-rimmed bodies, perfectly euhedral, isolated crystals of fluorapatite, pyrite and some ferruginized relicts of biotite, and even olivine, were observed. Although only present as cement, calcite spar is commonly the dominant mineral and has replaced in part more than 90% of the original minerals, including black-rimmed bodies and barite crystals, calcitic ghosts of which are common.

The contact of the purple limestone unit with the underlying cap dolostone is generally sharp and marked by a commonly erosional (Fig. 5d) hardground surface (Fig. 7a); however, its contact with the overlying cherts is clearly transitional and related to the absence of diagenetic cementation by calcite only and so we consider it to form the true base of the Ténigouri Group cherts and shales. In this regard, a recent study by Álvaro

et al. (in press), also recognises intercalations of limestone within basal cherts of the Ténigouri Group in some sections of the Atar Cliff area. Irregularities at the top of the cap dolostone, such as the domes described above, are blanketed by the Ténigouri Group; however, thin layers of bedded cherts appear locally within the upper part of the cap dolostone, while lenticular beds of dolostone can be present within the basal few metres of the Ténigouri Group.

4. Geochemical methods

Additional hand specimens were collected specifically for geochemical analysis during three separate field excursions in January 1997, December 1998 (Mauritania) and January 2002 (Mali). Petrographic thin-sections were studied for most samples, while selected barite and limestone samples were also investigated using X-ray diffractometry and scanning electron microscopy. Selected samples of barite were also prepared for the analysis of fluid inclusions, which are abundant in the barite specimens.

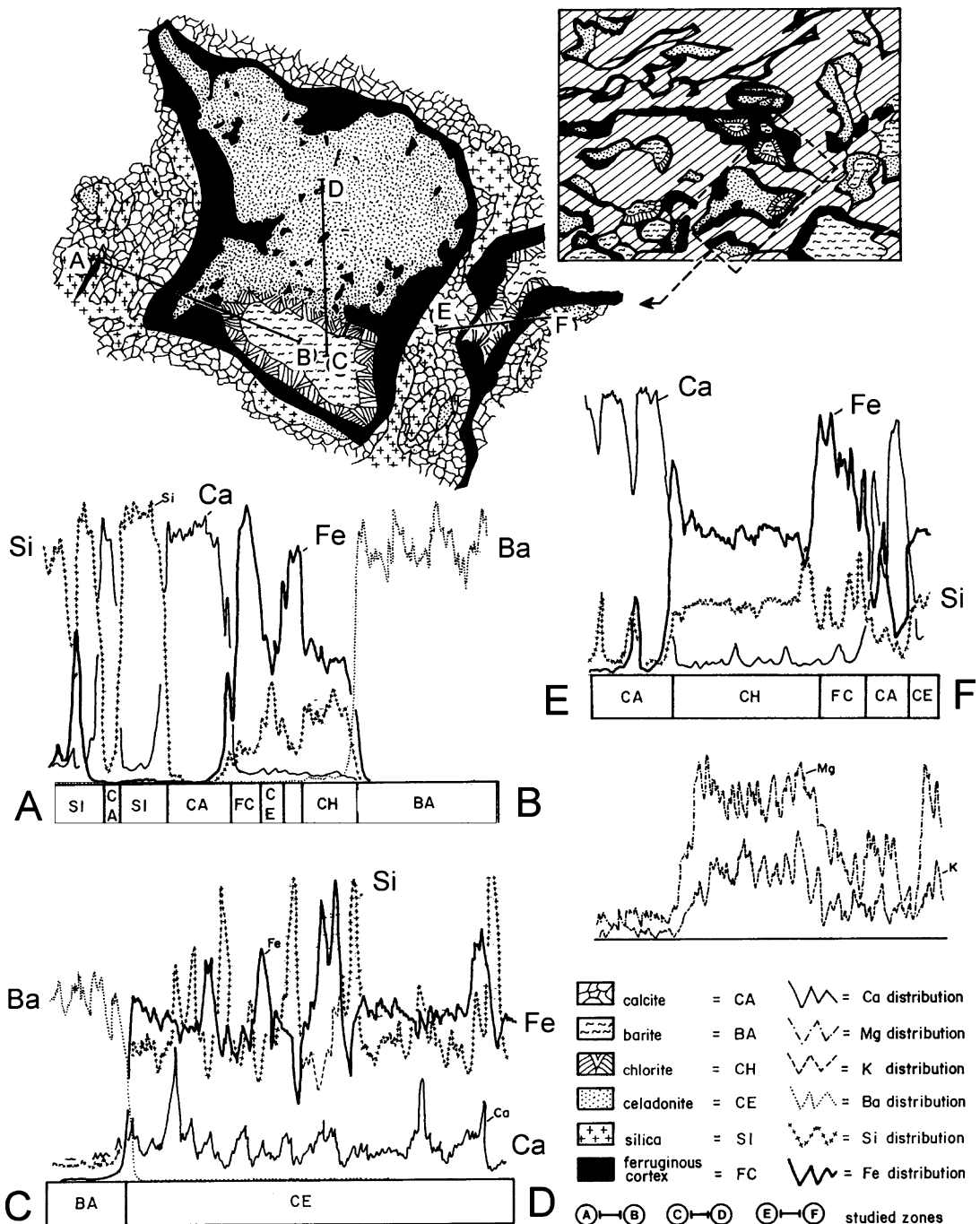


Fig. 9. Semi-quantitative microprobe analyses of a black-rimmed structure within the purple limestone horizon interpreted to be recrystallised volcanoclastic material.

Bulk carbonate carbon and oxygen isotope compositions (Tables 1–3; Fig. 3) were determined at the University of Oxford during 1997 courtesy of Martin Brasier and Julie Cartlidge. Samples were first cleaned with H_2O_2 and $(CH_3)_2CO$ and dried for 30 min at 60 °C before reaction with anhydrous phosphoric acid

at 90 °C using an on-line VG Isocarb system attached to a VG Isogas PRISM mass spectrometer. Delta values are reported relative to the international PDB standard. Calcite and dolomite inclusion stable isotope values pertain to work carried out at the Centre de Géochimie de la Surface (CNRS), Strasbourg by GS in 1998 (Table 4).

Table 1

Stable isotopic compositions of bulk carbonate rock powders from the Neoproterozoic Atar Group

Sample	Unit	Height (m)	d ¹³ C	d ¹⁸ O
Td19	I. 5	415	0.06	-10.021
Td18	I. 5	418	1.345	-7.933
Td17	I. 5	421	0.619	-10.688
Td16	I. 5	424	0.864	-7.043
Td15	I. 5	427	0.676	-10.135
Td14	I. 5	430	0.531	-10.331
Td13	I. 5	433	0.864	-9.734
Td12	I. 5	436	1.148	-9.748
Td10	I. 5	439	1.212	-8.816
Td9	I. 5	442	2.048	-5.885
Td8	I. 5	445	0.1	-10.431
Td7	I. 5	455	1.276	-9.781
Td6alt	I. 5	458	0.783	-8.851
Td5	I. 5	461	2.296	-8.107
Td4	I. 5	464	2.26	-5.331
Td3	I. 5	467	1.677	-6.433
Td2	I. 5	470	1.702	-8.5
OT19	I. 5/I. 6	520	4.789	-9.766
OT1	I. 6	540	-1.611	-10.323
OT2	I. 6	543	-1.706	-9.866
OT3	I. 6	546	-2.241	-10.928
OT4	I. 6	549	-2.029	-10.548
OT5	I. 6	552	-0.292	-9.364
OT6	I. 6	555	-1.673	-9.189
OT7alt	I. 6	560	-1.243	-8.212
OT8	I. 6	549	-1.852	-10.53
OT8b	I. 6	549	-1.603	-10.626
OT10	I. 6	570	-2.531	-9.826
OT11	I. 6	572	-2.484	-11.13
OT12	I. 6	573	-1.812	-8.674
OT13	I. 6	574	-2.18	-9.879
OT14	I. 6	580	-0.923	-9.518
OT15a	I. 6	576	2.32	-9.634
OT15b	I. 6	576	-2.4	-11.88
OT16	I. 6	538	-0.107	-9.95
OT17	I. 6	536	1.24	-8.783
Te1	I. 7	630	1.264	-8.264
Te2	I. 7	633	1.973	-8.721
Te3	I. 7	639	1.404	-8.621
Te4	I. 7	642	1.739	-6.719
Te5	I. 7	645	2.782	-8.018
Te6(g)	I. 7	648	1.821	-6.85
Te6(w)	I. 7	648	2.058	-7.806
Te7	I. 7	651	1.235	-5.273
Te8	I. 7	654	0.765	-8.143
Te9	I. 7	657	2.284	-7.134
Te10a(g)	I. 7	660	0.05	-3.825
Te10a(w)	I. 7	660	0.83	-5.907
Te10b(g)	I. 7	660	0.479	-5.935
Te10b(w)	I. 7	660	1.204	-6.726
Te11(g)	I. 7	663	0.211	-3.688
Te11(w)	I. 7	663	2.602	-7.59
Te12	I. 7	672	2.398	-6.854
Te13	I. 7	675	2.221	-6.823
Te14	I. 7	654	0.638	-9.122
Te15	I. 7	654	0.432	-9.337

Table 1 (Continued)

Sample	Unit	Height (m)	d ¹³ C	d ¹⁸ O
I7b(g)	I. 7	648	1.88	-7.286
I7b(w)	I. 7	648	1.342	-5.831
I7c(g)	I. 7	648	2.574	-7.033
I7c(w)	I. 7	648	2.12	-6.643
DB1	I. 9	725	1.631	-8.845
DB2	I. 9	728	1.524	-9.874
DB3	I. 9	729	1.112	-9.518
DB5	I. 9	732	1.738	-9.839
DB6	I. 9	735	1.698	-9.745
DB7	I. 9	738	1.692	-9.859
DB8	I. 9	740	1.769	-10.085
DB10	I. 9	750	0.992	-9.242
DB105	I. 9	750	1.147	-9.515
DB11	I. 9	763	1.262	-9.828
DB12	I. 9	765	1.415	-9.28
DB13	I. 9	767	0.77	-9.41
DB14	I. 9	769	1.542	-8.603
DB15	I. 9	770	1.397	-10.518
N3	I. 10	850	0.655	-7.319
GN34	I. 11	872	-1.347	-9.964
GN33	I. 11	874	-1.068	-9.406
GN32	I. 11	876	-0.961	-8.049
GN31	I. 11	878	-0.968	-9.273
GN30	I. 11	880	-0.776	-9.23
GN29	I. 11	882	-0.738	-7.835
GN28	I. 11	884	-0.08	-9.033
GN27	I. 11	886	-0.692	-8.089
GN27	I. 11	890	-0.946	-7.296
GN26	I. 11	892	-0.774	-9.582
GN25	I. 11	894	-0.555	-8.86
GN24	I. 11	896	-0.406	-7.186
GN23q	I. 11	898	-0.602	-9.484
GN22	I. 11	900	-0.91	-9.064
GN20	I. 11	902	-0.615	-9.524
GN19	I. 11	904	-0.354	-6.831
GN18	I. 11	906	-0.739	-11.394
GN17	I. 11	908	-0.243	-7.113
GN16	I. 11	910	-0.449	-6.586
GN14	I. 11	912	-0.352	-3.282
GN13	I. 11	914	-0.596	-4.199
GN12	I. 11	916	-0.496	-3.816
GN11	I. 11	918	-0.274	-3.694
GN10	I. 11	920	-0.869	-3.953
GN9	I. 11	922	-0.388	-3.354
GN8	I. 11	924	-0.625	-5.023
GN7	I. 11	926	-0.218	-3.923
GN7	I. 11	928	-0.443	-3.198
GN5	I. 11	930	-0.542	-3.407
GN4	I. 11	932	-0.604	-3.882
GN3	I. 11	934	-0.516	-3.904
GN2	I. 11	936	-0.196	-4.66
N1	I. 11	940	-0.89	-5.717
I3	I. 12	ca. 1000	1.53	-7.352

Due to the extremely flat topography of most sections, which necessitated sampling from multiple sections, stratigraphic heights are only approximations.

Samples were reacted with phosphoric acid offline at 60 °C overnight before analysis; delta values are reported relative to PDB. Additional bulk carbonate samples (Table 2) were prepared for analysis at the University of Saskatchewan, Canada by Tim Prokopiuk. Samples were roasted in a vacuum oven for 1 h at 200 °C to remove water and volatile organic contaminants before reaction with anhydrous phosphoric acid at 70 °C. Isotope ratios were corrected for acid fractionation and are reported relative to the V-PDB standard.

Barite samples were analysed for their Sr isotope compositions (Table 4) at the Centre de Géochimie de la Surface (CNRS), Strasbourg by GS during 1997. Several leaching techniques were applied because of the presence of carbonate, chert and the likely presence of small quantities of other contaminant minerals within the barite samples. Selected samples were leached with ammonium acetate solution buffered to a pH of approximately 4.5. Another mild leach was performed on some samples using 10% HBr as was a strong acid leach of 10% HNO₃. These various leaches resulted in significantly different values for the same samples, indicating that differential leaching of contaminant phases affected the results. Because of this inhomogeneity, a second HNO₃ leach was carried out on selected samples after all carbonate had been dissolved. It was demonstrated in a separate series of tests that both first and second leaches dissolved a small fraction of the barite, which being highly enriched in Sr, was easily sufficient for isotopic analysis and thus determines the measured Sr isotope ratio from the second leach. Sr isotopes were

analysed on a VG Sector multicollector (long-term mean NBS 987: 0.710254 ± 4, n = 73, 2S.E., and short-term mean: 0.710249 ± 6; n = 4, 2S.D.). An additional four samples were analysed commercially at ANTELLIS SARL in Toulouse, France. Samples were preleached in 10% nitric acid at room temperature during 24 h to remove carbonate minerals present as inclusions within the barite, followed by thorough rinsing in ultrapure water. Final leaching of the barite fraction for analysis was carried out using 10% nitric acid at 90 °C during 48 h. Analyses of the NBS standard SRM987 during the same sample run yielded 0.710243 (n = 2). Both laboratories produced standard values consistent with the generally accepted value of 0.710250.

Sulphur and oxygen isotope compositions of the barite samples were analysed using a Finnigan MAT DeltaPlus mass spectrometer at the University of Münster. Isotope values are reported relative to CDT and V-SMOW, respectively.

5. Geochemical results

Carbon isotope values ($\delta^{13}\text{C}$) of diverse components within the Jbeliat cap dolostone (Table 3) range widely between $-3.7\text{\textperthousand}$ and $+1.3\text{\textperthousand}$ (mean = $-2.0\text{\textperthousand}$; n = 13). Calcitic components within the overlying purple limestone unit are generally more enriched in ^{13}C , with values as high as $+3.8\text{\textperthousand}$ (mean = $+1.3\text{\textperthousand}$; n = 7). A thin, mostly silicified stromatolitic dolostone bed (calcaire d'Amogjar) within the lower part of the Atar Cliff Group yielded $\delta^{13}\text{C} = 0.3\text{\textperthousand}$ (n = 2). Oxygen iso-

Table 2
Stable isotopic compositions of cap dolostone units overlying evidence for glaciation in Mali

Sample	Location	Height (m)	Sample description	$\delta^{13}\text{C}$	$\delta^{18}\text{O}$
17/01/02.1	Koniakari	—	Dolomiticrite	-2.95	-7.76
17/01/02.2	Koniakari	—	Dolomiticrite	-3.67	-6.52
17/01/02.4	Koniakari	—	Dolomiticrite	-0.60	-6.19
17/01/02.5 base	Koniakari	0.1	Dolomiticrite	-2.68	-7.98
17/01/02.5 mid	Koniakari	0.5	Dolomiticrite	-3.81	-9.55
17/01/02.5 top	Koniakari	0.8	Dolomiticrite	-4.28	-8.67
18/01/02.1	Goumare	0.2	Dolosparite	-3.39	-6.82
18/01/02.1	Goumare	0.2	Dolosparite	-3.43	-6.78
18/01/02.3	Goumare	1	Dolosparite	-3.52	-9.05
18/01/02.4	Goumare	1.5	Dolosparite	-3.79	-5.39
18/01/02.4	Goumare	1.5	Dolomicrospar with acicular barite	-3.92	-5.74
18/01/02.5	Goumare	2.5	Dolosparite	-3.41	-6.50
18/01/02.6	Goumare	3	Dolospar growing in micritic calcite	-1.12	-6.56
18/01/02.10	Goumare	4.3	Dolomicrospar-spar	1.55	-5.07
18/01/02.12	Goumare	4.4	Dolomicrospar-spar	-0.37	-11.26
18/01/02.12	Goumare	4.4	Dolomicrospar-spar	2.79	-2.40

Data from Goumaré show a slight $\delta^{13}\text{C}$ decrease upsection before rising sharply to positive values at the top where there has been extensive silicification and brecciation (cf. Jbeliat data).

Table 3

Stable isotopic compositions of cap dolostones and higher carbonate unit (CO5) of the Jbeliat area, Adrar, Mauritania and upper cap samples from the Atar Cliff area

Sample	Location	Sample description	$\delta^{13}\text{C}$	$\delta^{18}\text{O}$
Cp2 Jb2a	Jbeliat (Section 2)	Sandy, coarse-grained dolospar sheet-crack fill (bedded cap)	-3.26	-5.96
Cp2 Jb2m	Jbeliat (Section 2)	Fine-grained, pinkish dolospar (bedded cap)	-3.72	-6.28
Cp2 Jb3	Jbeliat (Section 2)	Heavily veined, buff dolospar (bedded cap)	1.27	-5.90
Cp2 Jb4	Jbeliat (Section 2)	Pinkish, buff dolospar/microspar (bedded cap)	-3.85	-6.08
Cp2 Jb5	Jbeliat (Section 2)	Pinkish orange, coarse-grained dolospar (bedded cap)	-3.15	-5.90
Cp2 Jb6	Jbeliat (Section 2)	Pinkish orange, coarse-grained dolospar (bedded cap)	-2.33	-6.97
Cp2 Jb7	Jbeliat (Section 2)	Pinkish orange, coarse-grained dolospar (bedded cap)	-2.01	-8.23
Cp2 Jb9Qax	Jbeliat Section 2)	Very coarse-grained, pinkish grey dolospar (late cement)	-0.89	-8.67
Cp2 Jb10Q(x)	Jbeliat (Section 2)	Very coarse-grained, pinkish grey dolospar (late cement)	-1.13	-8.33
Cp2 Jb12	Jbeliat (Section 2)	Calcitised tuff breccia (purple limestone)	1.50	-6.85
Cp2 Jb13	Jbeliat (Section 2)	Calcitised tuff breccia (purple limestone)	-0.55	-8.66
Cp9 Jb1234	Jbeliat (Section 9)	Sandy dolostone with sheet cracks (bedded cap)	-3.10	-6.59
Cp9 Jb8	Jbeliat (Section 9)	Calcitised tuff breccia (purple limestone)	1.02	-8.19
Cp9 Jb10	Jbeliat (Section 9)	Nodular calcite facies (purple limestone)	3.78	-3.19
Cp10 Jb1	Jbeliat (Section 10)	Orange banded, coarse-grained dolospar (bedded cap)	-1.68	-7.00
Cp11 Jb2	Jbeliat (Section 11)	Calcitised tuff breccia (purple limestone)	2.29	-7.87
Cp11 Jb3	Jbeliat (Section 11)	Calcitised tuff breccia (purple limestone)	0.50	-6.81
Cp11 Jb3	Jbeliat (Section 11)	Calcitised tuff breccia (purple limestone)	0.43	-7.17
GNCO	Guelb Nouatil	Orange dolospar-cemented sandstone (upper cap)	-0.54	-3.58
N4	Guelb Nouatil	Orange dolospar-cemented conglomerate (upper cap)	-1.80	-7.23
CO5.5	Amogjar road	Base of silicified stromatolite at base of Atar Cliff Group	0.16	-6.29
CO5.2	Amogjar road	Top of silicified stromatolite at base of Atar Cliff Group	0.44	-7.09

'Bedded cap' refers to the relatively undisrupted layers, generally lower down in the cap dolostone. All dolomitic samples have been extensively recrystallised. Section numbers refer to Deynoux (1980).

Stable isotope values ($\delta^{18}\text{O}$) range between $-8.7\text{\textperthousand}$ and $-3.6\text{\textperthousand}$ (mean = $-6.7\text{\textperthousand}$; $n = 13$) within the cap dolostone, while the overlying purple limestone unit gave values between $-8.7\text{\textperthousand}$ and $-6.8\text{\textperthousand}$ (mean = $-7.6\text{\textperthousand}$; $n = 6$) with one outlier value at $-3.2\text{\textperthousand}$. Samples from the stromatolitic dolostone bed yielded $\delta^{18}\text{O} = -6.7\text{\textperthousand}$ ($n = 2$). Dolomite and calcite mineral inclusions incorporated within laminated barite mamelons of the cap dolostone exhibit similar $\delta^{13}\text{C}$ values to the cap dolostone (Table 4) ranging from $-3.5\text{\textperthousand}$ to $+0.2\text{\textperthousand}$ (mean = $-1.8\text{\textperthousand}$; $n = 11$) with dolomitic samples recording the lowest $\delta^{13}\text{C}$ values; however, $\delta^{18}\text{O}$ values range more widely between $-13.4\text{\textperthousand}$ and $-4.6\text{\textperthousand}$. Stable isotope values from the equivalent cap dolostone at Mali (Table 2) are similar in overall range and trend to those from Mauritania. $\delta^{13}\text{C}$ values at Goumaré begin negative around $-3.5\text{\textperthousand}$ with later and stratigraphically highest samples showing positive values. At Koniakari, the exposure was too poor to sample stratigraphically although one outcrop of less than a metre thickness shows a trend to more negative $\delta^{13}\text{C}$ values.

$\delta^{34}\text{S}$ values from barite at Jbeliat exhibit a remarkable range from $20.3\text{\textperthousand}$ to $45.6\text{\textperthousand}$ (mean = $27.1\text{\textperthousand}$; $n = 10$), similar to the range found in a smaller set of correlative barite samples from Mali (27.6 – $43.5\text{\textperthousand}$). Barite

$\delta^{18}\text{O}$ values range between $-20.0\text{\textperthousand}$ and $-16.9\text{\textperthousand}$ for a subset of seven samples of barite from Mauritania and Mali. $^{87}\text{Sr}/^{86}\text{Sr}$ ratios (Table 4) for barite samples from both Mauritania and Mali display a limited range (0.70773–0.70847) despite the diverse range of leaching techniques used to dissolve the barite and incorporated carbonate inclusions. In general, milder leaching techniques using weak acids resulted in more radiogenic $^{87}\text{Sr}/^{86}\text{Sr}$ ratios than with strong acid (HNO_3). Least radiogenic ratios (0.70773–0.70814) were obtained from the carbonate-free, second HNO_3 leach and ought to reflect the isotopic composition of the pure barite.

6. Discussion

6.1. Depositional environment and mineral paragenesis

The cap dolostones of the northern Taoudéni Basin mark an abrupt change in the local depositional environment from terrestrial to marine. The glacial formations consist of terrestrial tillites and proglacial outwash sandstones, which are capped in the Adrar region by a persistent horizon of large-scale polygonal structures and sand wedges. These polygonal structures are

Table 4

Geochemical compositions of barite samples and carbonate inclusions contained within them from cap dolostone units of Mauritania and Mali

Sample	Country	Locality	Section	Mineral	Mg/Ca ^{B/C}	% Carb.	$\delta^{13}\text{C}$	$\delta^{18}\text{O}$	$^{87}\text{Sr}/^{86}\text{Sr}^{\text{A}}$	$^{87}\text{Sr}/^{86}\text{Sr}^{\text{B}}$	$^{87}\text{Sr}/^{86}\text{Sr}^{\text{C}}$	$^{87}\text{Sr}/^{86}\text{Sr}^{\text{D}}$	$\delta^{34}\text{S}$	$\delta^{18}\text{O}$
CP2JB15	Mauritania	Jbéliat	2	Dol.	0.483	1.83	-3.2	-4.6	0.70791				31.4	
CP3JB4	Mauritania	Jbéliat	3	Dol.	0.296	0.67	-3.5	-6.0	0.70817					
CP9JB5	Mauritania	Jbéliat	9	Cal. + Dol.	0.097	4.22	-2.5	-12.8					23.3	
CP9JB6	Mauritania	Jbéliat	9	Cal. + dol.	0.056	0.93	0.2	-6.6	0.70799	0.70790	0.70785	0.70776		
CP9JB	Mauritania	Jbéliat	9	Cal. + dol.	0.068	1.7	-1.5	-12.3	0.70847	0.70819	0.70788	0.70780	45.6	
CP9.9	Mauritania	Jbéliat	9	Cal. + Dol.	0.112	0.94	-2.2	-13.4	0.70841	0.70787	0.70789			
CP9JB9	Mauritania	Jbéliat	9	Cal.	0.016	0.51	-1.9	-13.1	0.70836	0.70777	0.70789		25.5	
1547 (base)	Mauritania	Jbéliat	9	Cal.	0.020	1.89	-1.0	-11.8		0.70806		0.70773	28.3	19.3
1547 (top)	Mauritania	Jbéliat	9			—							23.3	18.0
CP9JB (B + C)	Mauritania	Jbéliat	9	Cal.	0.028	2.81	-0.9	-11.4				0.70794	22.3	16.9
1552 (base)	Mauritania	Jbéliat	9										29.5	17.9
1552 (top)	Mauritania	Jbéliat	9										20.3	
CP9JB2	Mauritania	Jbéliat	9											
CP15JB2	Mauritania	Jbéliat	15	Cal.	0.011	0.29	-0.7	-6.4						
CP36	Mauritania	Jbéliat	36	Dol.	0.281	0.16	-3.0	-10.5					21.4	
16.01.02.2	Mali	Kabaté	—									0.70814	43.5	20.0
16.01.02.3	Mali	Kabaté	—									0.70796	42.8	19.8
19.01.02.4	Mali	Kabaté	—										30.8	18.6
BA6 (HS)	Mali	Kabaté	—								0.70773*		27.6	

Regarding Sr isotope data: A: ammonium acetate leach (calcite + minor dolomite + minor barite fraction); B: HBr leach (calcite + dolomite + significant barite fraction); C: HNO_3 leach or $^{*}2.5\text{N HCl}$ (calcite + dolomite + significant barite + ?leached silicates fraction); D: second HNO_3 leach (barite only fraction). The lowest $^{87}\text{Sr}/^{86}\text{Sr}$ ratios for 11 samples are highlighted in bold text showing a small range (for barites) from 0.70773 to 0.70817, with most values 0.7077–0.7078.

evidence that a prolonged periglacial period with temperatures low enough for the development of permafrost (Deynoux, 1982) followed the retreat of glaciers in this part of the craton. Recent investigations by MD reveal that analogous polygonal structures and sand wedges can be found 500 km farther south in the Afollé Massif, south of Kiffa, indicating that permafrost was not restricted to the Adrar region but extended over a large part of the Taoudéni Basin.

The cap dolostones and overlying shales of the Ténigouri Group are considered to relate to deglacial to post-glacial eustatic transgression, respectively. However, the presence of intervening shales and sandstones levelling paleorelief (see above) as observed in the Adrar and Hank regions, highlights the complexity of this transgression. According to Aït-Kaci Ahmed and Moussine-Pouchkine (1994), and Bertrand-Sarfati et al. (1997), in the Hank Algerian border region (Guettatira-Grizim-Fersiga area), the cap carbonates and intervening shales, which contain intercalations of phosphatic grainstones, were deposited during the glacioeustatic transgression. Due to the balance between glacioeustatism and isostatic rebound, the cap carbonates were locally subjected on topographic highs to subaerial exposure with the development of a complex phosphatic profile, including ministromatolites, while sedimentation continued in the depressions. Intervening green shales pass progressively upward into sandy tidal deposits and eolian sandstones in the Hank. These sandstones are cut by a transgressive surface covered by a few metres of conglomeratic and phosphatic sandstones that preceded the large-scale development on the whole platform of shales equivalent to the Ténigouri Group in Mauritania.

Accordingly, the cap carbonates across the Taoudéni Basin may represent a condensed deposit that relates to the onset of the glacioeustatic transgression, with the transgressive and highstand system tracts preserved only in paleodepressions. A comparison can be made with the Late Ordovician glacial record on the Gondwana platform where the deposits from the glacioeustatic transgression are also sparsely preserved in paleodepressions, while the Silurian shales, like those of the Ténigouri Group, correspond to the restoration of normal, post-glacial subsidence of the platform (Ghienne, 2003). In this regard, we note that the recent ages for the Ténigouri Group (Lahondère et al., 2005) imply an approximately 20 million year interval between deglaciation and the deposition at higher levels within the Ténigouri Group (Fig. 3).

The brecciated facies occurs at various horizons within the cap dolostone and does not show any sys-

tematic relationship with erosional structures, such as channel form. Instead, the observed progressive disruption of the beds (Fig. 5) suggests *in situ* formation. Internal folding of beds and tepee structures are best explained by expansion caused by early diagenetic carbonate cementation (Hoffman and Schrag, 2002) and/or the formation of evaporitic sulphate minerals. This suggests that the carbonate saturation state of the early diagenetic environment was unusually elevated and/or that the basin was periodically restricted with respect to the global ocean. Because such features are common around the world in basal Ediacaran cap dolostones (Hoffman and Schrag, 2002; Shields, 2005) it seems likely that carbonate cementation caused by oversaturation was a major factor.

As in the Hank, the cap dolostone of the Adrar reveals a complex, relative sea-level record with the purple limestone representing a condensation horizon that marks the beginning of a second, marine transgression, apparently coinciding with regional volcanism. Residual flakes of isotropic or only faintly anisotropic material, generally preserved by an envelope of calcite marine cement (Fig. 8a and c), represent a primary volcaniclastic constituent of the rock. Microprobe analyses (Fig. 9) indicate that this material likely comprises poorly crystallised silica gel. The black-rimmed and iron-rich bodies that are found within this amorphous material exhibit forms, such as shards and rounded particles that are reminiscent of the iron- and silicate-rich glass characteristic of volcanic tuffs. The allophanes, green clay-minerals and other secondary products found within the black-rimmed bodies appear to support such a hypothesis; celadonite, for example, is considered to be one of the first-formed products during the recrystallisation of volcanic glass (Schlocker and Van Horn, 1958).

It seems unlikely that the small, needle-thin, commonly doubly terminated crystals of barite (Fig. 8b) could have survived the high energy environment that led to the deposition of an edgewise flake breccia (Fig. 8a). Therefore, barite in the purple limestone must be an authigenic, diagenetic mineral, which is consistent with the presence of rare, mm-wide barite veins seen in thin-section. Barite crystals within the volcanically influenced, purple limestone bed could therefore indicate a volcanic source for the barium. In this regard, barite monocrystals and polycrystalline mosaics are also seen in the interiors of black-rimmed bodies where barite replaces the volcanogenic minerals chlorite and celadonite. Locally, nests of automorphic albite are associated with this barite as are attapulgites, authigenic quartz, fibrous silica and a possible zeolite mineral (lau-monitite). Despite their association, barite precipitation

was clearly early and preceded the deposition of the overlying, and partly volcaniclastic Ténigouri Group. Isotopic arguments below further exclude the alteration of volcanogenic material as a controlling factor in barite genesis.

Calcite spherulites are found in two contexts within the cap carbonate succession. Firstly, they are found directly above a hardground that overlies a peneplaned, tepee-disrupted surface at the top of the cap dolostone (Fig. 7a). Secondly, they can also be found filling barite-coated, presumably karst-derived caverns (Fig. 6c) within the cap dolostone. In both cases, the spherulite level is clearly analogous to the purple limestone bed, and was similarly formed by the nucleation of calcite in a high-energy marine environment around siliceous, volcaniclastic debris, in this case amorphous, greenish fragments of altered glass. These relationships confirm that regional volcanism was coincident with marine transgression after palaeotopographic highs had for a time become emergent allowing karst dissolution to develop. Calcite saturation levels were high enough to grow calcite crystals rapidly on and in caverns immediately beneath the seafloor before glassy debris could disintegrate.

6.2. Carbonate isotope interpretations

Stable isotope compositions of the Jbeliat cap carbonate (Table 3) range widely but systematically. The earliest-formed components of the cap dolostone, represented by the brecciated, fine-grained, pinkish dolostone, form an isotopically distinct grouping with low $\delta^{13}\text{C}$ values down to $-3.8\text{\textperthousand}$ (Fig. 3) and consistent $\delta^{18}\text{O}$ values around $-6\text{\textperthousand}$. These values probably represent our closest approximation to the original isotopic composition of the Jbeliat cap dolostone. Similar values are also found in two samples of dolomite associated with barite specimens (Table 4) and seem characteristic of NW African cap dolostones in general (Porter et al., 2004; Shields et al., in press). Underlying carbonate units from the Atar Group exhibit significantly different $\delta^{13}\text{C}$ values (Fig. 3) that lie entirely outside the range of the cap dolostones. This indicates that microcrystalline dolomite did not derive from the reworking of underlying beds as has been postulated for dolomite above and within Neoproterozoic glaciogenic units of Scotland and elsewhere (Fairchild, 1993; Brasier and Shields, 2000).

Carbonate inclusions from barite within the upper levels of the cap dolostone at Jbeliat also show a range of $\delta^{13}\text{C}$ from $-3.5\text{\textperthousand}$ to positive values with the lowest values deriving from dolomite samples (Table 4). Sample CP2JB15, for example, exhibits a stable isotope compo-

sition identical to that of microsparitic dolostones from the same succession. Higher $\delta^{13}\text{C}$ values are associated with calcite, which is consistent with the pattern in the cap carbonate unit as a whole. However, $\delta^{18}\text{O}$ values of the calcite inclusions range widely from values similar to bulk values ($-6.4\text{\textperthousand}$) down to $-13.4\text{\textperthousand}$. Such $\delta^{18}\text{O}$ depletion could result from the influence of meteoric waters or higher temperatures or both (Marshall, 1992). Convincing covariation between $\delta^{13}\text{C}$ and $\delta^{18}\text{O}$ in barite samples from Section 9 (Deynoux, 1980) at Jbeliat (Table 4) indicates that the fluids responsible for the calcite inclusions underwent considerable isotopic evolution.

Table 2 shows additional C-isotope data from the cap dolostone horizon in Mali, which is associated at both localities with only minor barite mineralisation. At Koniakari, the cap is represented by a 0.8-m thick, centimeter-bedded, relatively undisrupted, mechanically laminated unit that shows a progression in $\delta^{13}\text{C}$ values from $-2.7\text{\textperthousand}$ to $-4.3\text{\textperthousand}$, identical to the trend reported from the Volta Basin (Porter et al., 2004). Carbonate associated with barite at Koniakari has a higher $\delta^{13}\text{C}$ value of $-0.6\text{\textperthousand}$. By contrast, at Goumaré, likewise in Mali, the cap dolostone is represented by 4.5 m of section with the top marked by a hardground, flooding surface underlain by reddened chert and disrupted beds. $\delta^{13}\text{C}$ values decrease slightly upsection from $-3.4\text{\textperthousand}$ to $-3.9\text{\textperthousand}$ in pink, well-bedded, physically laminated dolostones before rising again towards the top as at Jbeliat to more positive values as high as $+2.8\text{\textperthousand}$ in white-buff dolostone with tepee-like buckling, coarser sparry beds and widespread chert veins and silicification.

Heavily recrystallised samples of cap dolostone spar from Jbeliat, and samples from the upper cap dolostone unit, show rather higher and more variable $\delta^{13}\text{C}$ values, not generally typical of cap dolostone horizons elsewhere in the basin or worldwide and we attribute this to later isotopic exchange during recrystallisation, and the possible derivation of some of the carbonate material in the sandy and conglomeratic upper cap dolostone from erosion of the underlying Atar Group (cf. Álvaro et al., in press). Other late carbonate components, such as the calcite cement of the overlying purple limestone horizon, also exhibit unusually positive $\delta^{13}\text{C}$ values (cf. Hoffman and Schrag, 2002). If such values reflect a change in global seawater $\delta^{13}\text{C}$, then this would imply that the purple limestone was deposited sometime after the prominent post-glacial negative excursion, which has been documented worldwide (Kennedy et al., 1998). This interpretation is favoured by the authors and is explored further below. Alternatively, these values may have been elevated either by diagenesis, and possibly methanogenesis (e.g. Jiang et al., 2003) or through basi-

nal restriction. This latter explanation appears unlikely considering the additional Sr- and S-isotopic arguments below and the observation that the Ténigouri Group represents a regionally widespread, transgressive unit.

6.3. Carbon isotope stratigraphy

The Jbeliat sections and that at Goumaré are not amenable to detailed chemostratigraphic study because of multiple phases of cementation and recrystallisation as well as their vertical stratigraphic complexity, including multiple surfaces of hiatus, erosion and dissolution. Nevertheless, existing C-isotope results can be fitted convincingly into both a regional and a global context. A recent study of the presumably correlative cap dolostone of the SW Taoudéni Basin in the Walidiala Valley, Senegal reports a mean $\delta^{13}\text{C}$ value of $-3.9\text{\textperthousand}$ ($n=48$), and $\delta^{18}\text{O}$ of $-6.3\text{\textperthousand}$ with a stratigraphic trend towards more negative values (Shields et al., in press) that is not obvious in our comparatively small dataset from Jbeliat. Porter et al. (2004) published similarly depleted $\delta^{13}\text{C}$ and $\delta^{18}\text{O}$ values from cap dolostones of the neighbouring Volta Basin (Burkina Faso and Togo) also showing a clear trend towards more negative values. Further afield, Kennedy (1996) reports very similar results and decreasing trend from several “Mari-noan” (presumably Nuccaleena Formation-equivalent) cap dolostones in Australia. A similar trend is also found in the work of Halverson et al. (2004) from NE Svalbard, in which $\delta^{13}\text{C}$ ($-4\text{\textperthousand}$ to $-3\text{\textperthousand}$) and $\delta^{18}\text{O}$ ($-6\text{\textperthousand}$ to $-5\text{\textperthousand}$) values are virtually indistinguishable from those of dolomitic components in our study. The remarkable consistency of all these studies confirms a 635 Ma-age (Condon et al., 2005) for the Taoudéni Basin cap dolostones, and supports the assumption that all such draping cap dolostones are globally correlative (Kennedy et al., 1998; Knoll et al., 2006; Shields, 2005).

If we consider the Taoudéni Basin cap dolostone to be correlative with other ca. 635 Ma post-glacial units around the world, then overlying limestone units would normally be expected to exhibit even lower $\delta^{13}\text{C}$ values of around $-5\text{\textperthousand}$ (cf. Hoffman and Schrag, 2002), followed by a recovery to positive values upsection. The lack of carbonate rocks in the Ténigouri Group and the likelihood of time gaps within the triad at Jbeliat are consequently problematic. However, we note that Álvaro et al. (in press) report a stratigraphic trend through limestones of the basal 6 m of the Ténigouri Group in the Atar Cliff area from $-6\text{\textperthousand}$ to $+3.7\text{\textperthousand}$. We propose therefore that the thin (<50 cm) purple limestone of the Jbeliat area is a highly condensed unit equivalent to the 6 m of alternating cherts and limestone from one

section of the Atar Cliff area analysed for the Álvaro et al. study. Additionally, we tentatively consider the Ténigouri Group limestones to be correlative with other post-glacial, post-cap-dolostone limestones, such as the Maieberg Formation of northern Namibia (Hoffman et al., 1998). This global correlation is given further support below from isotopic studies of the barites from Jbeliat (Mauritania) and Pont de Kabaté (Mali).

6.4. Barite isotope interpretations

Strontium isotopes: The general consistency of our barite Sr isotope compositions (0.70773–0.70814) from geographically distant locations within the Taoudéni Basin is unusual for barites (Maynard et al., 1995). This consistency indicates that the mineralising fluids were isotopically homogeneous with respect to Sr despite the regionally widespread but localised nature of the barite mineralisation. Leaching experiments reveal that the lowermost values more faithfully correspond to the barite Sr component, with the spread in data related to impurities in the barite. Lowest values for $^{87}\text{Sr}/^{86}\text{Sr}$ (0.7077–8) are particularly consistent and indicate that the mineralising fluid was ultimately derived from seawater, the only plausible basin-scale homogeneous source. Identical $^{87}\text{Sr}/^{86}\text{Sr}$ ratios have been reported from Ediacaran successions worldwide (Shields, 1999; Pokrovskii et al., 2006; Halverson et al., in press), confirming further the early Ediacaran age of Taoudéni Basin cap dolostones and barites.

In their review of Neoproterozoic $^{87}\text{Sr}/^{86}\text{Sr}$ data, Halverson et al. (in press) report $^{87}\text{Sr}/^{86}\text{Sr}$ ratios from just above the cap dolostone level in NW Canada and N Namibia that are slightly lower (0.7071–2) than the barite $^{87}\text{Sr}/^{86}\text{Sr}$ values reported here (0.7077–8). The Namibian data then rise to 0.7080 during the recovery in $\delta^{13}\text{C}$ from its negative peak at the base of the Maieberg Formation. By comparison with the relatively rapid rise in seawater $^{87}\text{Sr}/^{86}\text{Sr}$ during the Cenozoic, such a shift of 0.0008 would not normally be expected to occur within a time frame shorter than 10 million years, which would imply that the barites from our study precipitated several million years after deglaciation. Assuming that these Sr isotope constraints both reflect ambient seawater, and have not been altered significantly, there are two additional possibilities, i.e. (1) that the oceans may not have been chemically homogeneous with respect to Sr during the post-glacial period (e.g. Shields, 2005; Hurtgen et al., 2006). In this regard, we note though that similarly low $^{87}\text{Sr}/^{86}\text{Sr}$ values (0.7072–3) have recently been published for post-glacial limestones of southern Siberia (Pokrovskii et al., 2006). Or (2) that global seawater

$^{87}\text{Sr}/^{86}\text{Sr}$ rose more rapidly than usual following end-Cryogenian glaciation due to elevated rates of chemical weathering (cf. Hoffman et al., 1998; Halverson et al., in press). This second possibility may turn out to be correct if we consider a slight discrepancy between the three well-defined Sr curves from Namibia, Canada and Siberia.

In the Pokrovskii et al. (2006) study, low values of 0.7072–3 were recorded from strata within the post-glacial negative $\delta^{13}\text{C}$ excursion as well as in presumably younger strata with extremely high $\delta^{13}\text{C}$ values. The climb in $^{87}\text{Sr}/^{86}\text{Sr}$ values to those of our barites, i.e. 0.7077–8, is therefore associated with highly negative $\delta^{13}\text{C}$ values only in the Halverson et al. (in press) study

but with highly positive $\delta^{13}\text{C}$ values in the Pokrovskii et al. (2006) study. These considerations permit the interpretation that there were two rises in seawater $^{87}\text{Sr}/^{86}\text{Sr}$ during the Ediacaran Period (Fig. 10), with a rapid rise after deglaciation (Halverson et al., in press) followed by a return to lower values before climbing again. Our barite deposits would appear to be associated with the first such rise, which followed immediately after deglaciation, as they are associated with the post-glacial negative $\delta^{13}\text{C}$ excursion. In any case, our $^{87}\text{Sr}/^{86}\text{Sr}$ data confirm the above-proposed, $\delta^{13}\text{C}$ -based correlation of the basal Téniagouri Group with other post-glacial limestones around the world.

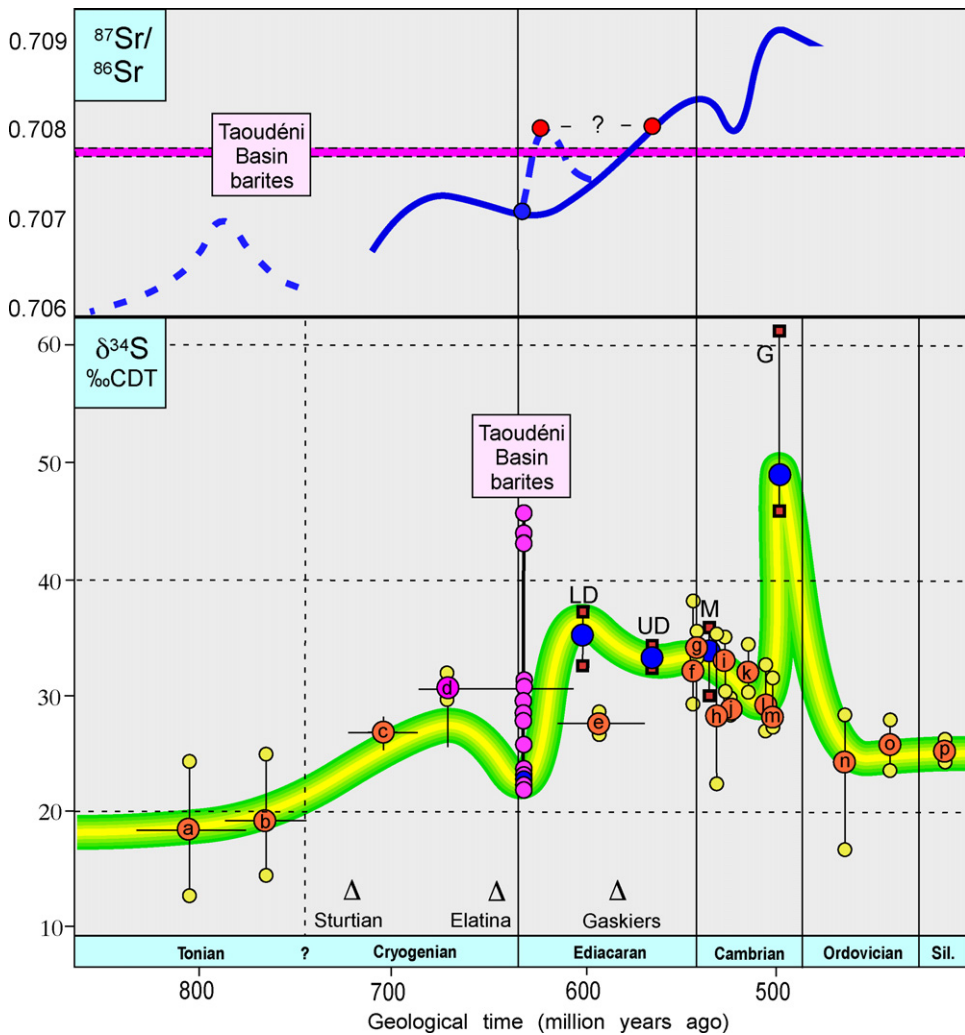


Fig. 10. Evolution of marine sulphate $\delta^{34}\text{S}$ during the Neoproterozoic–Paleozoic interval of Earth history based on published compilations (Hough et al., 2006) and this study. Mean values are shown as lettered circles (all evaporite-based data except for Misi and Veizer, 1998, where the mean (d) refers to stratiform, pyrite-free barite samples only), large circles (phosphate-associated sulphate data), while small circles show all the barite values from this study. Vertical bars represent the overall data range for each individual study. The interpreted seawater sulphate $\delta^{34}\text{S}$ curve is based on mean values and the constraints from barite herein (Fig. 12). Barite Sr isotope ratios (top figure) cross the Ediacaran seawater Sr curve between one and three times depending on whether two published rises to 0.708 (red circles) correlate or not, see text for explanation.

Sulphur isotopes: The sulphur isotopic compositions of the analysed barites range widely both at Jbeliat and in Mali, showing a total range of values between 20‰ and 46‰. Such high $\delta^{34}\text{S}$ values support the $^{87}\text{Sr}/^{86}\text{Sr}$ data in that they are consistent with a marine source for the sulphate in the barite. The fact that considerable isotopic differences exist even within the same sample mean that this range is unlikely to reflect fluctuations in seawater $\delta^{34}\text{S}$ but indicate instead that there was considerable sulphur isotope fractionation during modification of the primary seawater source. By comparison with other stratiform barite studies and modern sedimentary barite, the lowermost $\delta^{34}\text{S}$ values (~20‰) are most likely to reflect seawater $\delta^{34}\text{S}$ (Torres et al., 2003) because sulphate reduction, which is naturally associated with barium build-up in pore waters, tends to enrich the sulphate reservoir in ^{34}S . Examples of this tendency are reviewed in Jewell (2000) and Clark et al. (2004). For example, Devonian barite rosettes from Nevada (Clark et al., 2004) exhibit a large spread of $\delta^{34}\text{S}$ values between 29‰ and 56‰. Laminated and massive barites from the same study showed a smaller range between 21‰ and 29‰ with lowermost values closely corresponding to the S-isotopic composition of Devonian seawater, which is estimated to have been 20–25‰ (Kampschulte and Strauss, 2004). Modern methane seep-related barite is very similar in this regard, ranging in $\delta^{34}\text{S}$ from 21.6‰ to 67.4‰; modern day seawater $\delta^{34}\text{S}$ is about 21‰ (Kampschulte and Strauss, 2004). Consequently, our barites can potentially be used to constrain ambient seawater $\delta^{34}\text{S}$ (Fig. 10) to about 22–23‰.

Oxygen isotopes: Sulphate reduction will also modify the oxygen isotope composition of sulphate in the marine sulphate reservoir. Barite $\delta^{34}\text{S}$ and $\delta^{18}\text{O}$ values covary in the Taoudéni Basin dataset, thus confirming that the lowest values most closely reflect the S-isotopic composition of the primary ocean sulphate reservoir (Fig. 11). Although $\delta^{34}\text{S}:\delta^{18}\text{O}$ gradients should normally be 4:1 for sulphate reduction in nature (Clark and Fritz, 1997), one of the gradients in our study ranges higher although the number of samples and sample pairs is clearly not sufficient for a rigorous analysis. Lowermost $\delta^{18}\text{O}$ values of 17–18‰ in our study are consistent with published data from Neoproterozoic-Cambrian evaporites (Claypool et al., 1980; Strauss, 1993), while lowermost $\delta^{34}\text{S}$ values of 22–23‰ are consistent with published data from early Ediacaran marine sedimentary rocks elsewhere (Hurtgen et al., 2002, 2004, 2005). In particular, our constraint on seawater $\delta^{34}\text{S}$ of 22–23‰ is indistinguishable from reported $\delta^{34}\text{S}$ values (Hurtgen et al., 2006) from “open shelf” cap dolostones and post-glacial limestones of the southernmost Congo crato (northern Namibia) that were

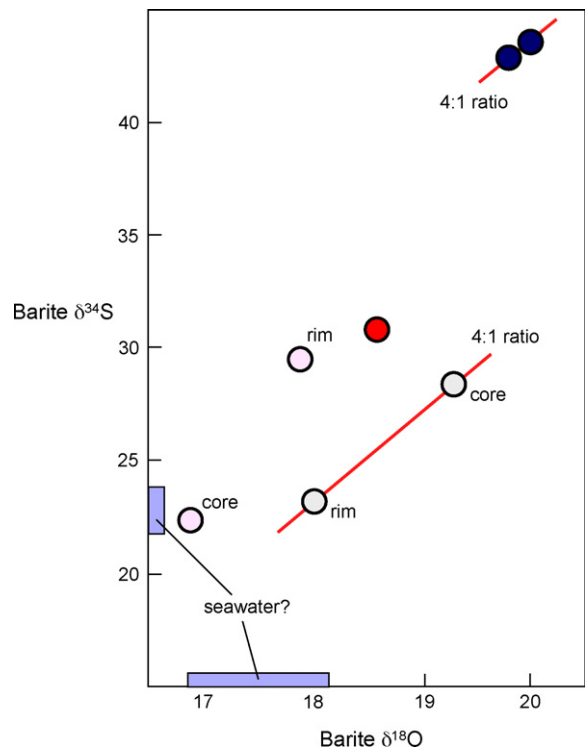


Fig. 11. Cross-plot showing S and O isotope ratios of barite samples from Jbeliat, Mauritania (open circles) and Pont de Kabaté, Mali (filled circles). Sulphate reduction ought to result in an isotopically heavier sulphate reservoir with a ratio of 4:1, shown by two of our sample pairs. The lowest $\delta^{34}\text{S}$ values of about 22–23‰ are therefore likely to be the least affected by sulphate reduction and should represent close, maximal approximations to the barite sulphate source, i.e. seawater.

deposited during the interval of negative $\delta^{13}\text{C}$ values and exhibit comparable $^{87}\text{Sr}/^{86}\text{Sr}$ ratios to those of our study (Halverson et al., in press). Higher $\delta^{34}\text{S}$ values are known from stratigraphically higher levels (after the $\delta^{13}\text{C}$ recovery) above the cap dolostone in South China (Shields et al., 2004), thus implying a major increase in seawater $\delta^{34}\text{S}$ during the early Ediacaran (Fig. 10).

6.5. Barite genesis

Marine barite forms today by three processes, which exhibit characteristic isotopic signatures: (1) hydrothermally, (2) biogenically and (3) diagenetically within organic-rich sediments as concretions and/or at cold methane seeps (Fig. 12). Barite may precipitate directly from barium-enriched hydrothermal fluids at submarine venting sites where Ba-bearing, reduced fluids meet ocean sulphate. Such barite deposits are commonly associated with anhydrite and polymetallic sulphides and exhibit mantle $\delta^{34}\text{S}$ values, i.e. about 0‰, and $^{87}\text{Sr}/^{86}\text{Sr}$ ratios that reflect the path taken by the mineral-

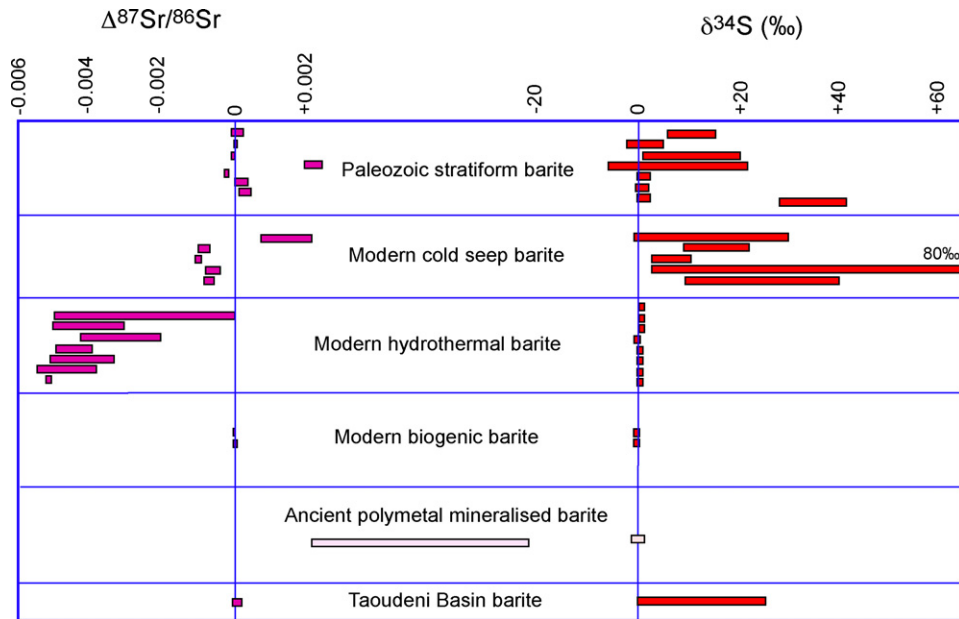


Fig. 12. Strontium and sulphur isotopic compositions of barite from this and published studies expressed as differences from contemporaneous seawater updated from Torres et al. (2003) with open boxes symbolically expressing published data in Maynard et al. (1995). Taoudéni Basin isotope compositions are characteristic for stratiform barite and are typical for cold methane seep deposits of the modern marine environment. Palaeozoic data have been adjusted to take into account more recent constraints on contemporaneous seawater $^{87}\text{Sr}/^{86}\text{Sr}$ and $\delta^{34}\text{S}$. Extremely high $\delta^{34}\text{S}$ values up to 80‰ are from seep-related barite in the Deryugin Basin (Okhotsk Sea) (Derkachev et al., 2000; Greinert et al., 2002).

ising fluids. Hydrothermal barite from spreading ridges and ridge flanks typically yield the low $^{87}\text{Sr}/^{86}\text{Sr}$ ratios characteristic of ocean crust (Torres et al., 2003), while intracratonic rift barite, which often contains economic quantities of Pb and Zn, exhibits highly radiogenic $^{87}\text{Sr}/^{86}\text{Sr}$ ratios (Maynard et al., 1995). The Taoudéni Basin barite is stratigraphically very restricted, contains no additional metal enrichments, has Sr- and S-isotope compositions that both show marine influence, and lacks a Eu anomaly in barium-free ICP-MS REE analyses (Shields, unpublished data), all of which seems to place it more in the category of stratiform or bedded barite (Maynard et al., 1995; Jewell, 2000) and rules out any significant hydrothermal (or volcanogenic) influence.

Much stratiform barite derives initially from biogenic barite, which is thought to precipitate (possibly replacing acantharian SrSO_4 tests) within the oxygen minimum zone of the water column and forms a common, but minor constituent of most pelagic sediments today. Primary biogenic barite exhibits the Sr- and S-isotopic characteristics of the seawater in which it precipitated (Fig. 12). Because barite is easily reduced within the sulphate reducing zone, purely biogenic barite is uncommon in sedimentary rocks. However, biogenic barium may build up within the zone of methanogenesis beneath areas of high productivity due to a combination of barium release during organic decay and microbially mediated

reduction of biogenic barite. Diagenetic barite nodules formed in this way may be preserved in the rock record, presumably during episodes of high organic productivity and low sedimentation rate. Such recycled biogenic barite (diagenetic barite) will bear the characteristic isotopic signature of sulphate reduction, which enriches the sulphate reservoir in ^{34}S and ^{18}O . It is unknown whether skeletally derived biogenic barite was present in the Precambrian ocean, but in any case the Taoudéni Basin barite is neither concretionary nor associated with organic-rich strata, and so is unlikely to have formed from the recycling of organic matter and biogenic barite during diagenesis.

Diagenetically recycled barite can also precipitate at vent sites on the seafloor along continental margins where fluids enriched in recycled diagenetic barium and hydrocarbons meet seawater sulphate. This may occur at faults or in areas of deep scouring where the zone of methanogenesis becomes exposed. Modern cold seep barite yields a wide range of $\delta^{34}\text{S}$ values, from seawater $\delta^{34}\text{S}$ upward (Fig. 12), which reflects bacterial reduction of seawater sulphate generally coupled with methane oxidation. Methanogenesis, a process that generally occurs after sulphate reduction has reached completion, is associated with barium enrichment because barite is highly soluble in the absence of sulphate. Cold methane seep barite today is therefore found at sites where

methane-bearing fluids bypass the sulphate-reducing zone and enter directly into sulphate-bearing seawater (Torres et al., 2003). Our Sr- and S-isotopic data from Taoudéni Basin barite match those of both modern, cold methane seep barite as well as ancient, stratiform barite deposits, which are interpreted to have formed from methane seeps (Torres et al., 2003). In the absence of organic-rich strata as a methane source, Ba may have been sequestered during oxidation of methane seeping from methane hydrates within the underlying permafrost that had formed during an extended period of exposure (Deynoux, 1982). The seemingly firm relationship between significant barite deposits on the West African craton and terrestrial periglacial facies is consistent with this scenario.

If barite was indeed related to methane hydrate decomposition, then barite precipitation coincided with the thawing of submerged permafrost deposits on the West African craton. That temperatures were frigid at the start of cap dolostone deposition is already indicated by the perfect preservation of permafrost features such as patterned ground (Deynoux, 1982) during rapid marine transgression, while the constraints indicated above imply that cap dolostone deposition bracketed this thawing phase. It is possible therefore that the entire cap dolostone in the Taoudéni Basin was deposited during a still cool interval, which only began to be relieved during the second marine transgression. Such an interpretation implies rapid deposition of the cap dolostone, which is central to hotly debated cap dolostone precipitation mechanisms (Grotzinger and Knoll, 1995; Hoffman et al., 1998; Kennedy et al., 2001; Shields, 2005) and supports the common interpretation that depositional breaks within the cap dolostone relate to isostatic reequilibration (lithosphere rebound) caused by ice retreat (e.g. James et al., 2001).

Isotopic considerations imply that two fluids were involved in the Taoudéni Basin case: a sulphate- and strontium-rich fluid (seawater) and a highly reducing, barium- and possibly methane-rich (but strontium-poor) fluid, which derived from within or below the level of the cap dolostone. Features such as doming are consistent with groundwater seepage, in which case exhalative fluids might derive ultimately from the regional flow of groundwater, possibly from the exposed Reguibat Shield to the north; however, the source of the mobilised Ba is hard to ascertain. Given the stratigraphic restriction of the barite, the Ba flux is unlikely to have lasted for a long time and so might be expected also to be restricted stratigraphically, possibly originating in porewaters within the post-glacial pile. Some models of the aftermath of end-Cryogenian glaciation invoke anoxic and extremely

sulphate-poor oceans during glaciation and deglaciation (Hoffman and Schrag, 2002; Shields, 2005; Hurtgen et al., 2006), in which case barite might have precipitated directly from seawater and remobilised porewaters following reinvigoration of the oxidative sulphur cycle during the early Ediacaran. In this regard, barite is not only known from cap carbonate sequences in NW Africa but also from S. China, where it is associated with C-isotopic evidence for methane seepage (Jiang et al., 2003), NW Canada (Hoffman and Schrag, 2002) and other localities worldwide (various personal communication). Barite in cap dolostones across the Taoudéni Basin and worldwide occurs systematically at the sharp boundary between dolomitic and calcitic units of cap carbonate successions (Shields, 2005). Given the well known inhibiting effect that sulphate ions have on dolomite precipitation (Baker and Kaster, 1981), this observation is consistent with a change from a sulphate-poor to a sulphate-rich marine environment following deglaciation.

6.6. Sequence of post-glacial events in the Taoudéni Basin

The succession of post-glacial depositional events and inferred sea-level changes in the Adrar region are outlined in Fig. 13. They are generally the same as those identified by Bertrand-Sarfati et al. (1997) from the Hank region further to the northeast (Fig. 1), which possesses a similar suite of terrestrial, periglacial and glacial facies (Deynoux, 1980). The post-glacial record of the Adrar region is also compatible with inferred sea-level changes reported by Shields et al. (in press) from a glaciomarine setting in the southeastern part of the basin. In that study, the nearshore, hemipelagic setting experienced a relative sea-level fall after regional deglaciation, which was interpreted to relate to isostatic rebound, with cap dolostone deposition beginning only later during a subsequent marine transgression.

The complexity of post-glacial deposition across the Taoudéni Basin suggests strongly the combined influences of isostatic rebound and glacioeustatic sea-level rise due to melting of ice sheets. An alternative interpretation that the relative sea-level falls seen here and elsewhere in the Taoudéni Basin (Bertrand-Sarfati et al., 1997; Shields et al., in press) correspond to renewed glaciation is not favoured here because correlative cap dolostones worldwide show no evidence for ice rafted debris after the initial, deglacial, marine transgression. The isotopic evidence presented above indicates that both the dolostone and overlying limestones in the Adrar region relate to the cap carbonate package of Hoffman and Schrag (2002).

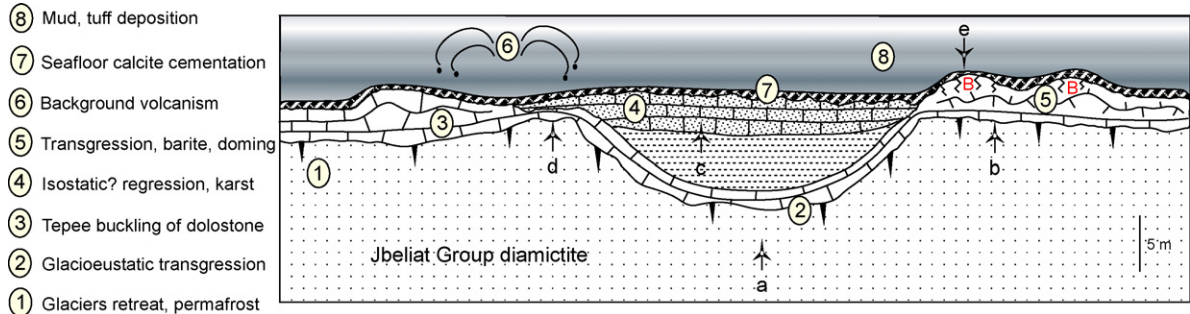


Fig. 13. Schematic interpretation of the inferred sequence of events in the Atar Cliff area (left) to the Jbeliat area (right) of the Taoudéni Basin, Mauritania. Events 6 and 8 are likely to be continuous rather than restricted in time. B refers to major barite occurrences. Letters a–e refer to figured successions in the article: a = Fig. 4d; b = Fig. 5a and c; c = Fig. 7c and d; d = Figs. 5b and d and 7a and b; e = Figs. 6a and c–e and 8a.

The sequence of events illustrated in Fig. 13 is also given briefly here: (1) local glacier retreat, permafrost development and subaerial deposition across the Taoudéni Basin. (2) Global deglaciation, glacioeustatic transgression, inundation by seawater and deposition of a thin veneer of dolomite powder (cap dolostone). (3) High degree of supersaturation in porewaters and seawater, dolomite cementation, buckling and fitted brecciation of beds. If Ba ultimately derived from seawater, then it was possibly sequestered in the sediment pile during this initial transgression directly from seawater and/or through the alteration of volcaniclastic material within the intermediate shales. (4) Relative sea-level fall related to the balance between eustatic rise and isostatic rebound, deposition in troughs of siliciclastic material that coarsens up into cross-bedded sandstones and conglomerates. True tepee-style buckling, karstic dissolution of dolostone beds on highs. (5) Second marine transgression related possibly to the outpacing of local isostatic rebound by global sea-level rise. Groundwater seepage to the seafloor results in localised barite precipitation in cavities, fissures and directly on the seafloor. (6) Volcaniclastic influence is maintained throughout this transgressive phase and continues into the strata above. (7) Volcanic clasts are cemented directly on the seafloor by calcite (steps 5–7 are semi-contemporaneous). (8) Continued deposition of bedded cherts and shales across the entire region due to restored subsidence of the basin.

7. Conclusions

A thin, transgressive cap dolostone unit drapes exquisitely preserved, glacial and periglacial landscapes along the margins of the Taoudéni Basin in NW Africa. Facies associations are complex as the initial marine transgression was followed by relative sea-level fall and periods of subaerial exposure, possibly related to isostatic rebound of the lithosphere after glacial retreat.

Continuation of the marine transgression inundated the Taoudéni Basin during an episode of widespread volcanic activity across the craton. The seepage of methane- and Ba-rich fluids through the cap carbonate succession exploited and contributed further to the disruption of dolostone beds and led to localised barite deposition during this second marine transgression, which was also associated with calcite cementation of the seafloor. The close association between relative sea-level changes, glacier retreat and cap dolostone deposition across the Taoudéni Basin implies that the cap dolostones here formed largely over a period of $\sim 10^4$ years, the maximum length of time over which isostatic rebound is likely to be significant. The systematic stratigraphic position of barite between dolomitic and calcitic beds in cap carbonate successions here and worldwide indicates that an increase in seawater sulphate content in post-glacial surface seawater may have been the overriding control on barite supersaturation.

Acknowledgements

This project benefited greatly from very detailed and constructive reviews from two anonymous reviewers. This publication is a contribution to ECLIPSE project “Proterozoic global climatic and environmental changes” and IGCP 512 project “Neoproterozoic Ice Ages”. We gratefully acknowledge expert analytical assistance and advice from P. Stille and B. Kieffel (Strasbourg), J. Cartlidge (Oxford), T. Prokopiuk (Saskatoon).

References

- Ait-Kaci Ahmed, A., Moussine-Pouchkine, A., 1994. Les formations cambriennes de Fersiga (Sud-Ouest du Tanezrouft): Nouvelle interprétation de la sédimentation glaciaire et post-glaciaire sur le Craton Ouest Africain. Bulletin du Service géologique d’Algérie 5 (1), 3–21.

- Álvaro, J.J., Macouin, M., Bauluz, B., Clausen, S., Ader, M., 2007. The Ediacaran sedimentary architecture and carbonate productivity in the Atar Cliffs, Adrar, Mauritania: palaeoenvironments, chemostratigraphy and diagenesis. *Precambrian Res.* 153, 236–261.
- Baker, P.A., Kaster, M., 1981. Constraints on the formation of sedimentary dolomite. *Science* 213, 214–216.
- Bertrand-Sarfati, J., Trompette, R., 1976. Use of stromatolites for intrabasinal correlation: example from the Late Proterozoic of the Northwestern margin of the Taoudeni Basin. In: Walter, M.R. (Ed.), *Stromatolites*. Elsevier, Amsterdam, pp. 251–259.
- Bertrand-Sarfati, J., Moussine-Pouchkine, A.Q., Amard, B., Aït Kaci Ahmed, A., 1995. First Ediacaran fauna found in western Africa and evidence for an Early Cambrian glaciation. *Geology* 23, 133–136.
- Bertrand-Sarfati, J., Flicoteaux, R., Moussine-Pouchkine, A., Aït Kaci Ahmed, A., 1997. Lower Cambrian apatitic stromatolites and phospharenites related to the glacio-eustatic cratonic rebound (Sahara, Algeria). *J. Sediment. Res.* 67 (5), 957–974.
- Brasier, M.D., Shields, G.A., 2000. Chemostratigraphy and correlation of the Neoproterozoic Port Askaig glaciation, Dalradian Supergroup of Scotland. *J. Geol. Soc. (Lond.)* 157, 909–914.
- Clark, I.D., Fritz, P., 1997. *Environmental Isotopes in Hydrogeology*. CRC Press LLC, p. 328.
- Clark, S.H.B., Poole, F.G., Wang, Z., 2004. Comparison of some sediment-hosted, stratiform barite deposits in China, the United States, and India. *Ore Geol. Rev.* 24, 85–101.
- Clauer, N., 1976. Géochimie isotopique du strontium des milieux sédimentaires. Application à la géochronologie de la couverture du craton ouest-africain. *Sciences Géologiques Mémoires*, Strasbourg 45, 256.
- Clauer, N., Caby, R., Jeanette, D., Trompette, R., 1982. Geochronology of sedimentary and metasedimentary Precambrian rocks of the West African Craton. *Precambrian Res.* 18, 53–71.
- Clauer, N., Deynoux, M., 1987. New information on the probable isotopic age of the Late Proterozoic glaciation in West Africa. *Precambrian Res.* 37, 89–94.
- Claypool, G.E., Holser, W.T., Kaplan, I.R., Sakai, H., Zak, I., 1980. The age curves of sulfur and oxygen isotopes in marine sulfate and their mutual interpretation. *Chem. Geol.* 28, 199–260.
- Condon, D., Zhu, M., Bowring, S., Wang, W., Yang, A., Jin, Y., 2005. U–Pb ages from the Neoproterozoic Doushantuo formation, China. *Science* 308, 95–98.
- Crawford, A.R., Daily, B., 1971. Probable non-synchronicity of late Precambrian glaciations. *Nature* 230, 111–112.
- Crowell, J.C., 1983. Ice ages recorded on Gonwanan continents. *Trans. Geol. Soc. S. Afr.* 86, 262–273.
- Culver, S.J., Hunt, D., 1991. Lithostratigraphy of the Precambrian–Cambrian boundary sequence in the southwestern Taoudeni Basin, West Africa. *J. Afr. Earth Sci.* 13, 407–413.
- Culver, S.J., Pojeta, J., Repetski, J.E., 1988. First record of Early Cambrian shelly microfossils from West Africa. *Geology* 16, 599–695.
- Derkachev, A.N., Bohrmann, G., Greinert, J., Mozherovskii, A.V., 2000. Authigenic carbonate and barite mineralization in sediments of the Deryugin Basin (Sea of Okhotsk). *Lithol. Miner. Resour.* 35, 504–519.
- Deynoux, M., 1980. Les formations glaciaires du Précambrien terminal et de la fin de l'Ordovicien en Afrique de l'Ouest. Deux exemples de glaciation d'inlandsis sur une plate-forme stable. *Trav. Lab. Sci. Terre St-Jérôme, Marseille (B)* 17, 554.
- Deynoux, M., 1982. Periglacial polygonal structures and sand wedges in the late Precambrian glacial formations of the Taoudeni Basin in Adrar of Mauritania (West Africa). *Palaeogeogr. Palaeoclimat. Palaeoecol.* 39, 55–70.
- Deynoux, M., 1985. Terrestrial or waterlain glacial diamictites? Three case studies from the Late Precambrian and Late Ordovician glacial drifts in West Africa. *Palaeogeogr. Palaeoclimat. Palaeoecol.* 51, 97–141.
- Deynoux, M., Trompette, R., 1976. Late Precambrian mixites: glacial and/or nonglacial? A discussion dealing especially with the mixites of West Africa. *Am. J. Sci.* 276, 1302–1315.
- Deynoux, M., Trompette, R., 1981. Late Precambrian tillite of the Taoudeni Basin West Africa. In: Hambrey, M.J., Harland, W.B. (Eds.), *Earth's Pre-Pleistocene Glacial Record*. Cambridge University Press, New York, pp. 123–134.
- Deynoux, M., Trompette, R., Clauer, N., Sougy, J., 1978. Upper Precambrian and lowermost Palaeozoic correlations in West Africa and in the western part of Central Africa Possible diachronism of Late Precambrian tillite. *Geol. Rundschau* 67, 615–630.
- Deynoux, M., Affaton, P., Trompette, R., Villeneuve, M., 2006. Pan-African tectonic evolution and glacial events registered in Neoproterozoic to Cambrian cratonic and foreland basins of West Africa. *J. African Earth Sci.* 46, 397–426.
- Evans, D.A.D., 2000. Stratigraphic, geochronological, and paleomagnetic constraints upon the Neoproterozoic climatic paradox. *Am. J. Sci.* 300, 347–433.
- Eyles, N., Januszczak, 2004. Zipper-rift": a tectonic model for Neoproterozoic glaciations during the breakup of Rodinia after 750 Ma. *Earth Sci. Rev.* 65, 1–73.
- Fairchild, I.J., 1993. Balmy shores and icy wastes: the paradox of carbonates associated with glacial deposits in Neoproterozoic times. *Sediment. Rev.* 1, 1–16.
- Fairchild, I.J., Marshall, J.D., Bertrand-Sarfati, J., 1990. Stratigraphic shifts in carbon isotopes from Proterozoic stromatolitic carbonates (Mauritania): influences of primary mineralogy and diagenesis. *Am. J. Sci.* 290A, 46–79.
- Ghienne, J.F., 2003. Late Ordovician sedimentary environments, glacial cycles, and post glacial transgression in the Taoudeni Basin, Ouest Africa. *Palaeogeogr. Palaeoclimat. Palaeoecol.* 189, 117–145.
- Girard, J.P., 1985. Diagenèse hydrothermale tardive des sédiments grésio-argileux du Protérozoïque supérieur du bassin de Taoudeni (Afrique de l'Ouest). Unpublished Thesis. Univ. Poitiers, 250 pp.
- Girard, J.P., Deynoux, M., Nahon, D., 1989. Diagenesis of the Upper Proterozoic siliciclastic sediments of the Teoudeni Basin (West Africa) and relation to diabase emplacement. *J. Sediment. Petrol.* 59, 233–248.
- Greinert, J., Bollwerk, S.M., Derkachev, A., Bohrmann, G., Suess, E., 2002. Massive carbonates and barite mineralization in the Derugin Basin (Sea of Okhotsk): precipitation processes at cold seep sites. *Earth Planet. Sci. Lett.* 203, 165–180.
- Grotzinger, J.P., Knoll, A.H., 1995. Anomalous carbonate precipitates: is the Precambrian the key to the Permian? *Palaios* 10, 578–596.
- Halverson, G.P., Maloof, A.C., Hoffman, P., 2004. The Marino an glaciation (Neoproterozoic) in northeast Svalbard. *Basin Res.* 16, 297–324.
- Halverson, G.P., Dudas, F., Maloof, A.C., Bowring, S.A. Evolution of the $^{87}\text{Sr}/^{86}\text{Sr}$ composition of Neoproterozoic seawater. *Palaeogeogr. Palaeoclimat. Palaeoecol.*, in press.
- Harland, W.B., 1964. Critical evidence for a great Infra-Cambrian glaciation. *Geol. Rundschau* 54, 45–61.
- Hoffman, P.F., Kaufman, A.J., Halverson, G.P., Schrag, D.P., 1998. A Neoproterozoic snowball earth. *Science* 281, 1342–1346.

- Hoffman, P.F., Schrag, D.P., 2002. The snowball earth hypothesis: testing the limits of global change. *Terra Nova* 14, 129–155.
- Hough, M.L., Shields, G.A., Evans, L.Z., Strauss, H., Henderson, R.A., Mackenzie, S., 2006. A major sulphur isotope event at c 510 Ma: a possible anoxia-extinction. Volcanism connection during the Early-Middle Cambrian transition? *Terra Nova* 18, 257–263.
- Hurtgen, M.T., Arthur, M.A., Suits, N.S., Kaufman, A.J., 2002. The sulphur isotopic composition of Neoproterozoic seawater sulphate: implications for a snowball Earth? *Earth Planet. Sci. Lett.* 203, 413–429.
- Hurtgen, M.T., Arthur, M.A., Prave, A.R., 2004. The sulfur isotope composition of carbonate-associated sulfate in Mesoproterozoic to Neoproterozoic carbonates from Death Valley, California. In: Amend, J.P., Edwards, K.J., Lyons, T.W. (Eds.), *Sulfur Biogeochemistry: Past and Present*. Geol. Soc. Amer. Special Paper, vol. 379, pp. 177–194.
- Hurtgen, M.T., Arthur, M.A., Halverson, G.P., 2005. Neoproterozoic sulfur isotopes, the evolution of microbial sulfur species, and the burial efficiency of sulfide as sedimentary pyrite. *Geology* 33, 41–44.
- Hurtgen, M.T., Halverson, G.P., Arthur, M.A., Hoffman, P.F., 2006. Sulfur cycling in the aftermath of a 635-Ma snowball glaciation: Evidence for a syn-glacial sulfidic deep ocean. *Earth Planet. Sci. Lett.* 245, 551–570.
- James, N.P., Narbonne, G.M., Kyser, T.K., 2001. Late Neoproterozoic cap carbonates: Mackenzie Mountains, northwestern Canada: precipitation and global glacial meltdown. *Can. J. Earth Sci.* 38, 1229–1262.
- James, N.P., Narbonne, G.M., Dalrymple, R.W., Kyser, T.K., 2005. Glendonites in Neoproterozoic low-latitude, interglacial, sedimentary rocks, northwest Canada: Insights into the Cryogenian ocean and Precambrian cold-water carbonates. *Geology* 33, 9–12.
- Jewell, P.W., 2000. Bedded barite in the geological record. In: Glenn, C.R., et al. (Eds.), *Marine Authigenesis: From Global to Microbial*, vol. 66. SEPM Spec. Publ., pp. 147–161.
- Jiang, G., Kennedy, M.J., Christie-Blick, N., 2003. Stable isotopic evidence for methane seeps in Neoproterozoic postglacial cap carbonates. *Nature* 426, 822–826.
- Kampschulte, A., Strauss, H., 2004. The sulfur isotopic evolution of Phanerozoic seawater based on analysis of structurally substituted sulfate in carbonates. *Chem. Geol.* 204, 255–286.
- Kennedy, M.J., 1996. Stratigraphy, sedimentology, and isotopic geochemistry of Australian Neoproterozoic postglacial cap dolostones: deglaciation, $\delta^{13}\text{C}$ excursions and carbonate precipitation. *J. Sediment. Res.* 66, 1050–1064.
- Kennedy, M.J., Runnegar, B., Prave, A.R., Hoffmann, K.-H., Arthur, M.A., 1998. Two or four Neoproterozoic glaciations? *Geology* 26, 1059–1063.
- Kennedy, M.J., Christie-Blick, N., Sohl, L.E., 2001. Are Proterozoic cap carbonates and isotope excursions a record of gas hydrate destabilization following Earth's coldest intervals. *Geology* 29, 443–446.
- Kilner, B., Mac Niocaill, C., Brasier, M.D., 2005. Low-latitude glaciation in the Neoproterozoic of Oman. *Geology* 33, 413–416.
- Knoll, A.H., Walter, M.R., Narbonne, G., Christie-Blick, N., 2006. The Ediacaran Period: a new addition to the geologic time scale. *Lethaia* 39, 13–30.
- Lahondère, D., Roger, J., Le Metour, J., Donzeau, M., Guillocheau, F., Helm, C., Thieblemont, D., Cochérie, A., Guerrot, C., 2005. Notice explicative des cartes géologiques à 1/200,000 et 1/500,000 de l'extrême sud de la Mauritanie. DMG, Ministère des mines et de l'industrie, Nouakchott, Rapport BRGM/RC-54273-FR, 610 pp.
- Leprun, J.-C., Trompette, R., 1969. Subdivision du Voltaïen du massif de Gobnangou (République de Haute-Volta) en deux séries discordantes séparées par une tillite d'âge éocambrien probable. *Comptes rendus de l'académie des sciences, Paris* 269, 2187–2190.
- Marshall, J.D., 1992. Climatic and oceanographic isotopic signals from the carbonate rock record and their preservation. *Geol. Mag.* 129, 143–160.
- Maynard, J.B., Morton, J., Valdes-Nodarse, E.L., Diaz-Carmona, A., 1995. Sr isotopes of bedded barites: guide to distinguishing basins with Pb-Zn mineralization. *Eco. Geol.* 90, 2058–2064.
- Misi, A., Veizer, J., 1998. Neoproterozoic carbonate sequences of the Una Group, Irene Basin, Brazil: chemostratigraphy, age and correlations. *Precambrian Res.* 89, 87–100.
- Pokrovskii, B.G., Melezhik, V.A., Bujakeite, M.I., 2006. Carbon, oxygen, strontium and sulphur isotopic compositions in late Precambrian rocks of the Patom complex, central Siberia: Communication 1. Results, isotope stratigraphy and dating problems. *Lithol. Miner. Resour.* 41, 450–474.
- Porter, A.M., Knoll, A.H., Affaton, P., 2004. Chemostratigraphy of Neoproterozoic cap carbonates from the Volta Basin, West Africa. *Precambrian Res.* 130, 99–112.
- Ridgwell, A.J., Kennedy, M.J., Caldeira, K., 2003. Carbonate deposition, climate stability, and Neoproterozoic ice ages. *Science* 302, 859–862.
- Rossi, P., 1982. Lithostratigraphie et cartographie des formations sédimentaires du pourtour du Massif du Kaarta, Mali Occidental. Précambrien inférieur (?) du Sud-Ouest du Bassin de Taoudéni. *Travaux des Laboratoires des Sciences de la Terre Série B* 18, 274.
- Schermerhorn, L.J.G., 1974. Late Precambrian mixtites: glacial and/or nonglacial. *Am. J. Sci.* 274, 673–824.
- Schlocker, J., Van Horn, R., 1958. alteration of volcanic glass near Denver, Colorado. *J. Sediment. Res.* 28, 31–35.
- Shields, G.A., 1999. Working towards a new stratigraphic calibration scheme for the Neoproterozoic–Cambrian. *Eclogae Geologicae Helvetiae* 92, 221–233.
- Shields, G.A., 2002. A chemical explanation for the mid-Neoproterozoic disappearance of molar-tooth structure ~750 Ma. *Terra Nova* 14, 108–113.
- Shields, G.A., 2005. Cap carbonates: a critical appraisal of existing formation models and the Plumeworld hypothesis. *Terra Nova* 17, 299–310.
- Shields, G.A., Kimura, H., Yang, J., Gammon, P., 2004. Sulphur isotopic evolution of Neoproterozoic–Cambrian seawater: new francolite-bound sulphate $\delta^{34}\text{S}$ data and a critical appraisal of the existing record. *Chem. Geol.* 204, 163–182.
- Shields, G.A., Deynoux, M., Culver, S.J., Brasier, M.D., Affaton, P., Vandamme, D., in press. Neoproterozoic glaciomarine and cap dolostone facies of the southwestern Taoudéni Basin (Walidiala Valley, Senegal/Guinea, NW Africa). *Comptes rendus de l'académie des sciences: geosciences*, doi:10.1016/j.crte.2006.10.002.
- Sohl, L.E., Christie-Blick, N., Kent, D.V., 1999. Paleomagnetic polarity reversals in Marinoan (ca. 600 Ma) glacial deposits of Australia: implications for the duration of low-latitude glaciation in Neoproterozoic time. *Geol. Soc. Am. Bull.* 111, 1120–1139.
- Spencer, A.M., 1971. Late Precambrian glaciation in Scotland. *Mem. Geol. Soc. Lond.* 6, 100.
- Spencer, A.M., Spencer, M.O., 1972. The Late Precambrian/Lower Cambrian Bonahaven Dolomite of Islay and its stromatolites. *Scott. J. Geol.* 8, 269–282.

- Strauss, H., 1993. The sulfur isotopic composition of Precambrian sulfates: new data and a critical evaluation of the existing record. *Precambrian Res.* 63, 225–246.
- Torres, M.E., Bohrmann, G., Dubé, T.E., Poole, F.G., 2003. Formation of modern and Paleozoic barite at continental margin methane seeps. *Geology* 31, 897–900.
- Trompette, R., 1973. Le Précambrien supérieur et le Paléozoïque inférieur de l'Adrar de Mauritanie (bordure occidentale du bassin de Taoudeni, Afrique de l'Ouest). Un exemple de sédimentation de craton, Etude stratigraphique et sédimentologique. *Trav. Lab. Sci. Terre St-Jérôme, Marseille (B)*, 7.
- Veizer, J., Compston, W., Clauer, N., Schidlowski, M., 1983. $^{87}\text{Sr}/^{86}\text{Sr}$ in Late Proterozoic carbonates: evidence for a “mantle” event at ~900 Ma ago. *Geochim. Cosmochim. Acta* 47, 295–302.
- Williams, G.E., 1975. Late Precambrian glacial climate and the earth's obliquity. *Geol. Mag.* 112, 441–465.
- Wilson, C.B., Harland, W.B., 1964. The Polarizbreen Series and other evidences of late pre-Cambrian ice ages in Spitsbergen. *Geol. Mag.* 101, 198–219.
- Young, G.M., 1976. Iron formation and glaciogenic rocks of the Rapitan Group, Northwest Territories, Canada. *Precambrian Res.* 3, 137–158.
- Zimmermann, M., 1960. Nouvelle subdivision des séries antégothlandiennes de l'Afrique occidentale (Mauritanie, Soudan, Sénégal). In: Rap. 21st Inter. Geol. Congr., vol. 8, Copenhagen, pp. 26–36.